Scientific Research Publishing

International Journal of Geosciences, 2022, 13, 382-413
https://www.scirp.org/journal/ijg
ISSN Online: 2156-8367
ISSN Print: 2156-8359

Comparative Geochemical and Petrographic Studies of the Various Granitoids between Central and Western Arm, in the Central Part of Ramagiri Schist Belt and Their Petrogenetic Histories

Eirin Kar, Prasun Ghosh, Shibani Mishra

State Unit Andhra Pradesh, Geological Survey of India, Southern Region, Hyderabad, India
Email: eirinkar75@gmail.com

How to cite this paper: Kar, E., Ghosh, P. and Mishra, S. (2022) Comparative Geochemical and Petrographic Studies of the Various Granitoids between Central and Western Arm, in the Central Part of Ramagiri Schist Belt and Their Petrogenetic Histories. *International Journal of Geosciences*, **13**, 382-413.
https://doi.org/10.4236/ijg.2022.135021

Received: April 23, 2022
Accepted: May 28, 2022
Published: May 31, 2022

Abstract

Granitoids between the central and western arm of Ramagiri schist belt in its central part, are broadly classified into the migmatite gneiss, grey granodiorite and pink monzogranite, based on field characteristics and petrographic features. These granitoids belong to the Tonalite-Granodiorite-Monzogranite (TGM) suite of PGC-II. All the samples are fresh as per the CIA values, PC1-PC2 binary plot and MFW ternary plot. The granodiorites occupy the expected field in the normative IUGS, TAS, and R_1-R_2 classification diagrams, but the monzogranites occupy the monzogranite field in the normative IUGS classification diagram and granite to alkali granite field in the rest. The granodiorites exhibit both ferroan to magnesian, alkali-calcic nature with metaluminous I type features and falls in the calc-alkaline to high K calc-alkaline series. They have high ΣREE (an average 327.905 ppm) content, and show LREE enrichment ($(La/Sm)_N$ = 3.1 - 6.8) with enriched but relatively flat HREE ($(Gd/Yb)_N$ = 1.75 - 5.26) patterns and weak negative to positive Eu anomaly (Eu/Eu* = 0.62 - 1.18). The monzogranites, on the other hand, are peraluminous, alkalic, ferroan, high K calc-alkaline, S-type granites, exhibiting relatively low ΣREE (an average 118.693 ppm) contents, strongly fractionated REE patterns with highly enriched LREE ($(La/Sm)_N$ =1.74 - 9.76), depleted HREE ($(Gd/Yb)_N$ = 0.43 - 2.21) patterns having concave upward shape, and strong negative Eu anomaly (Eu/Eu* = 0.23 - 0.89). Geothermobarometry revealed the average emplacement temperature and pressure of the granodiorites and monzogranites as 812.5˚C, 8.14 ± 0.6 kbar and 775˚C, 3.14 kbar, respectively. Based, on the observations, it can be concluded that the granodiorites have formed in volcanic arc setting by partial melting of the lower

crust and S-type monzogranites have been produced at a relatively shallower depth in the crust, by continental crust recycling due to hydrothermal influx.

Keywords

Ramagiri Schist Belt, Granodiorites, Monzogranites, Volcanic Arc

1. Introduction

Vast stretches of granites with high strain equivalent gneisses, enclosing narrow linear greenstone belts, represent the Archaean granite-greenstone terrain of eastern block of Dharwar craton (EDC). The important greenstone belts of EDC include the Ramagiri-Penakacherla-Hungund-Kushtagi superbelt, Kolar-Kadiri-Julakava-Jonnagiri-Hutti-Muski superbelt, Veligallu-Gadwal superbelt, Tsundupalli schist belt and Nellore-Khammam super belt. Recent studies indicated these greenstone belts as composite tectonostratigraphic terranes of accreted plume-derived and convergent margin-derived magmatic sequences [1]. Earlier workers revealed four magma suites in the EDC: 1) Tonalite-trondjhemite-granodiorite gneiss suite (TTG); 2) Trondjhemite-granodiorite-monzogranite (TGM) suite; 3) Monzosyenite-syenogranite (MS) suite; and 4) Granite and k-feldspar granite suite (AFGS) *i.e.* shear controlled post orogenic granites and anarogenic (A-type) granites [2]-[15].

The present study area is the central part of the trident-shaped Ramagiri supracrustal belt (RSB), surrounded on all sides by granitoid gneisses and intrusive granites. Tectonic mélange of basaltic and felsic bimodal lavas intermixed with minor amounts of clastic sediments defines the RSB. The trident shape of the belt is due to alternating high-level diapiric intrusion of granitoids and rocks of schist belt [16] [17] [18] [19].

Detailed petrographic and geochemical characterizations of the granitoids around Kadiri, Kolar, Velligallu, and Nellore schist belt have been done by different authors and the petrogenesis of these granitoids with respect to the overall genesis of the schist belts has been worked out. [13] grouped the granites and gneisses of Penakacherla schist belt into TTG, TGM and MS suites, based on their lithological association. They also, evaluated their structural, petrographic, petrochemical characteristics, mutual field relationships and relationship with the schist belt.

However, a comparative petro-chemical characterization of the granitoids in the central part of trident shaped RSB, specifically, of the granitoids between central and western arm of RSB, is yet to be done. Hence, the present work details the distribution, field relations, petrography and geochemistry of the granites and gneisses in the central part of RSB in and around Balepalyam and Ramagiri village. Detailed field and petrographic studies of the granitoids observed in the study area are first used to club them under the established magma suites as per IUGS scheme, followed by the genetical classification of the granitoids.

Also, emphasis has been given on the behavior of trace elements and REE of the various granitoids and geothermobarometry to determine their petrogenesis and their implication in bearing certain mineralization.

2. Geological Setting

The study area is confined to the granitoids occupying the area around the central and western arms of RSB in its central part near Ramagiri and Balepalyam village. The central arm of the RSB is comprised of mainly chlorite schist, carbonaceous chlorite schist and massive and foliated metabasalt. The western arm of the schist belt is comprised of pillowed metabasalt, chlorite schist, carbonaceous chlorite schist, banded iron formation, quartzite, and ultramafites. Dolerite/gabbro dykes traverse all the units occurring in the area. Further they were intruded by kimberlites, lamprophyres and granophyres. The two arms are surrounded by different phases of granitoids (**Figure 1**).

Mineralogical observations during the present study broadly revealed three categories of granitoids in the area: Migmatite gneiss, granodiorite and monzogranite. The granodiorites and monzogranites are further categorized as equigranular and porphyritic based on the textural properties of the granitoids. Granodiorites are gneissic at places. The present study mainly compares the field, petrographic and geochemical characteristics of the broad categories of granodiorites, monzogranites and migmatite gneiss, with special emphasis on the petrogenesis of granodiorites and monzogranites.

3. Distribution and Field Relations

Migmatite gneiss is grey, medium grained, mesocratic, defined by layers of melanosome and criss-cross patterned leucosomes (**Figure 2(a)**). These rocks show stromatic, ptygmatic and phlebitic structures. Melanosomes of the migmatite gneiss are comprised of fine to medium grained biotite (10%) and hornblendes (5%) while the leucosome part is mostly dominated by coarse grained quartz (30% - 35%), plagioclase (25% - 30%), k-feldspar (5% - 10%), and traces of magnetite, sphene, and pyrite (2%).

The granodiorites and monzogranites are spatially associated with each other and usually occur as vastly spread, large lenticular stocks. Granodiorites are mesocratic and grey colored with medium to coarse grained texture. The dominant mineralogy is quartz (20% - 25%), plagioclase (25% - 35%), and k-feldspar (12% - 15%), with subordinate amounts of hornblende (10%), biotite (2% - 3%) and traces of sphene and apatite. The rock occurs as both equigranular and porphyritic variety. Due to the equigranular mosaic of felsic and mafic minerals in the equigranular variety, the rock appears as salt and pepper texture (**Figure 2(b)**). The porphyritic granodiorites are characterized by large, lath-shaped plagioclase grains embedded in a groundmass of quartz, plagioclase, alkali feldspar and mafics (**Figure 2(c)**). The size of the phenocrysts varies from 0.5 cms to upto 3 cms. The monzogranites are weathered near the surface. The rock is recognized by its

flesh-pink color, leucocratic nature and medium to coarse crystals of k-feldspar (30% - 35%), quartz (25% - 30%), plagioclase (20% - 25%) and traces of biotite (5%) and apatite (**Figure 2(d)**, **Figure 2(e)**). K-feldspars occur as both large phenocrysts and groundmass. The k-feldspar phenocrysts are tabular, size varying from <5 mms to 5 cms and contain inclusion of sericitized plagioclase, biotite and granular quartz. This rock is devoid of synplutonic microgranitoid enclaves-dykelets. Arrangement of phenocrysts of feldspars in both granodiorites and monzogranites in a particular direction defines a crude magmatic foliation in the rock. The contact of the granodiorites and monzogranites with the schist belt is generally sharp and intrusive but tectonised at places due to later shearing (**Figure 2(f)**).

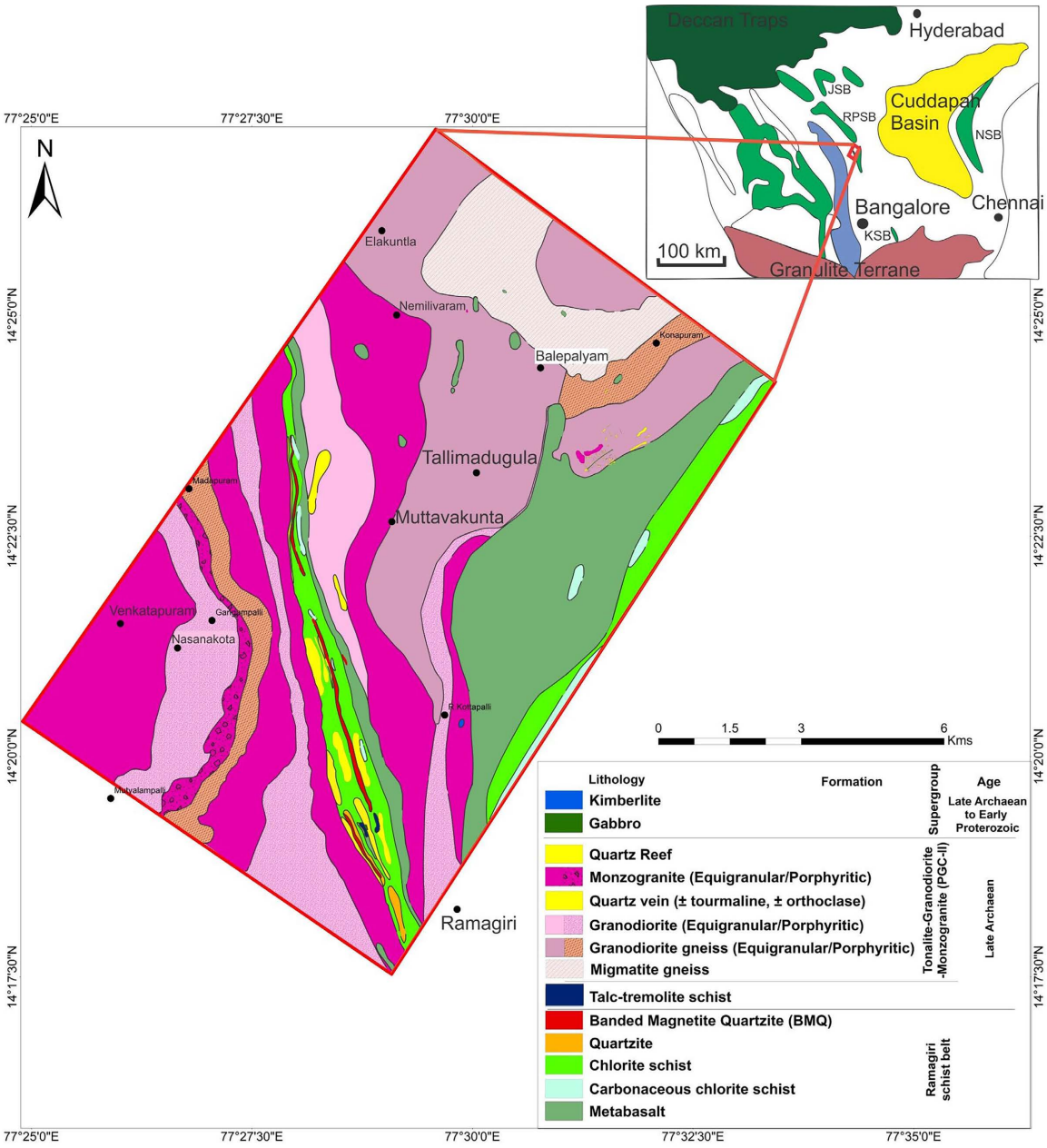

Figure 1. Geological map of the Ramagiri-Balepalyam area.

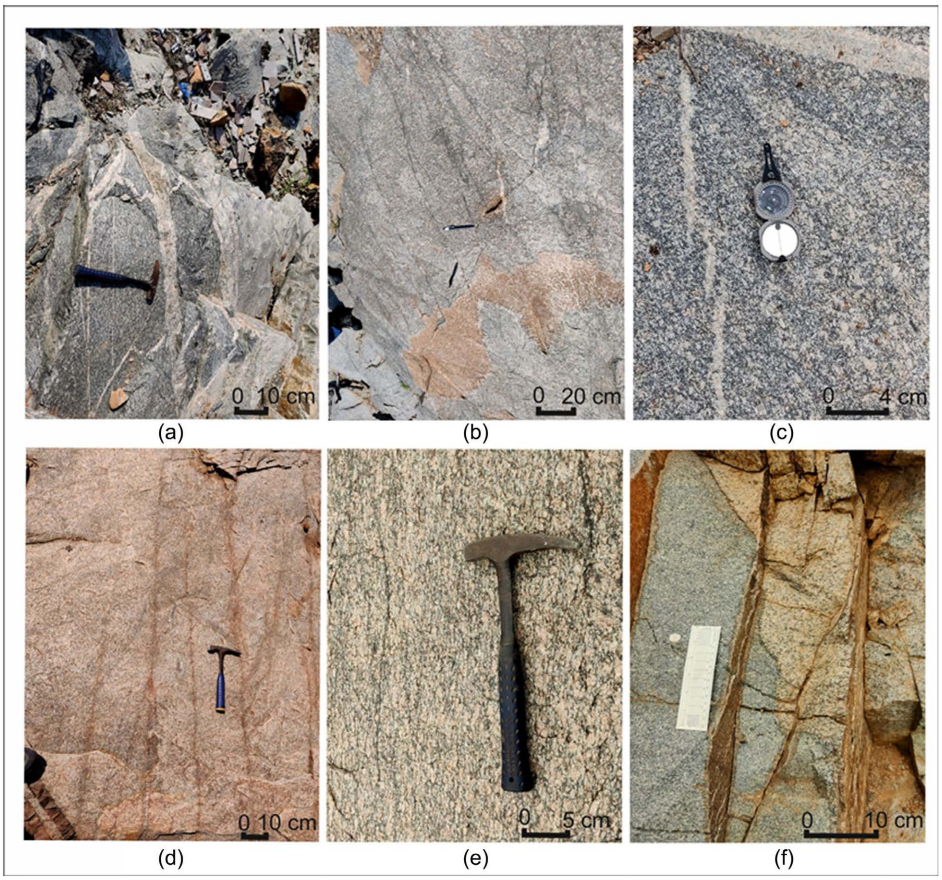

Figure 2. (a) Field exposure of migmatite gneiss; (b) Equigranular granodiorite; (c) Porphyritic granodiorite; (d) Equigranular monzogranite; (e) Porphyritic monzogranite; (f) Intrusive contact of granodiorite and monzogranite.

Presence of mafic microgranular enclaves (MME) is observed in all the three rocks (**Figure 3(a)**, **Figure 3(b)**). However, in the monzogranites, presence of both MME and small dyke like bodies of mafic rich microgranitoids and enclavial bodies (MMDs) is observed (Figure 3b). They are few meters in length and their intrusive nature is indicated by the angularity of the length of the dykes. Rapakivi texture is also observed very prominently in some of the plagioclase phenocrysts within the monzogranite, indicating magma mixing and mingling (**Figure 3(c)**).

Several gold and pyrite bearing quartz veins (±tourmaline, ±scheelite) are observed in the area within the monzogranites.

Enclaves of dominantly metabasalt and amphibolites of RSB are observed in all these three types of granitoids, indicating the granitoids occupying areas between the central and western arm and west of western arm of schist belt to be younger than the rocks of RSB, possibly belonging to the TGM suite of PGC-II.

4. Petrography

In thin section of migmatite gneiss, plagioclase is normally zoned and carries fine inclusions of sphene, apatite, zircon and rutile that lie in planes parallel to

long axes or the twin planes of these plagioclase crystals (Figure 4(a)). Alternately arranged mafic and felsic minerals produces the gneissic structure and granoblastic texture (Figure 4(b)). K-feldspar megacrysts show intensive perthitization of exsolution origin and some include xenomorphic quartz crystals between the idiomorphic cores and their outer rims (Figure 4(c)). Porphyritic, myrmekitic and graphic textures are common in these rocks (Figure 4(d)). Biotite and hornblende show alteration to chlorite and epidote. Plagioclase and potash feldspar show alteration to saussurite and kaolinite respectively. The above observations suggest that the rock was originally metamorphosed to amphibolite grade and subsequently underwent retrogression.

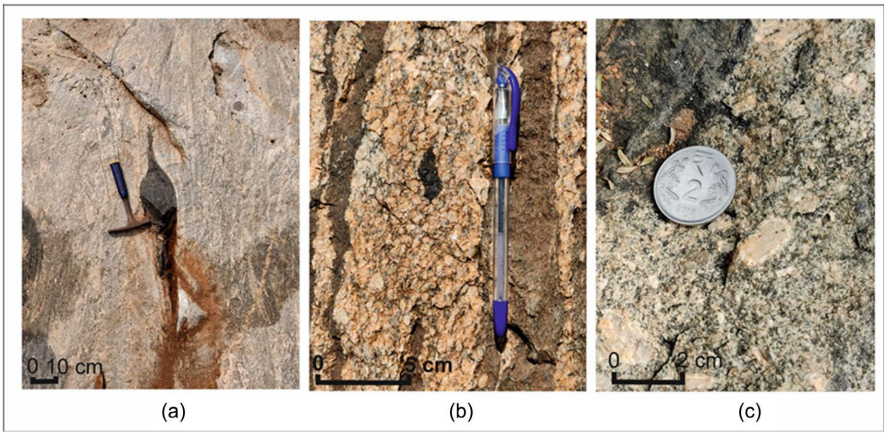

Figure 3. (a) Oblate MME within migmatite gneiss; (b) Synplutonic mafic micro granular enclavial dykes and sheared MME; (c) RAPAKIVI texture in monzogranite.

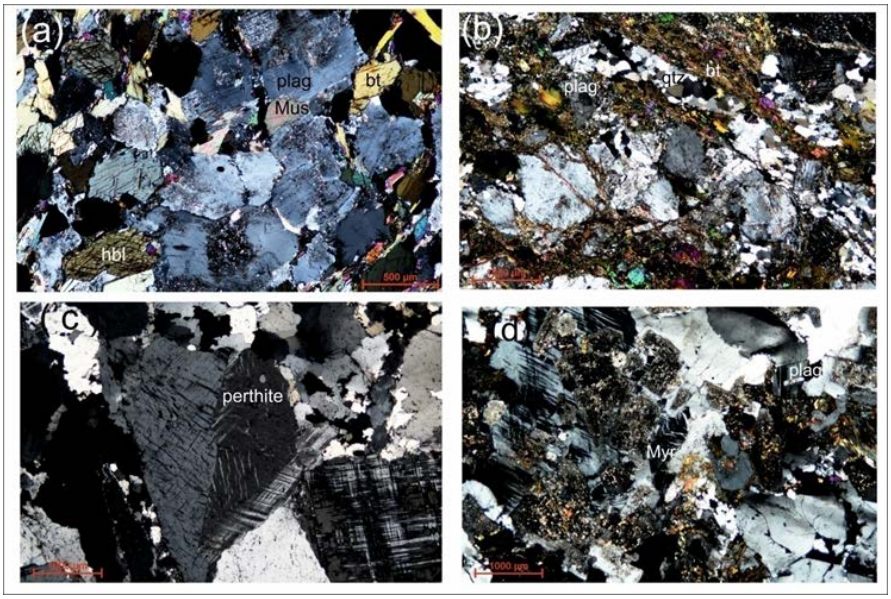

Figure 4. (a) Zoned plagioclases with fine inclusions of sphene, apatite, zircon and rutile in migmatite gneiss; (b) Alternately arranged mafic and felsic minerals defining gneissic and granoblastic texture in migmatite gneiss; (c) Perthite texture in monzogranites; (d) Myrmekite texture, sericitized plagioclase in migmatite gneiss. Plag: plagioclase; bt: biotite; mus: muscovite; hbl: hornblende; Qtz: quartz; per: perthite; Myr: myrmekite.

The granodiorites show holocrystalline, seriate to hypidiomorphic texture and essentially consists of quartz, plagioclase, biotite, hornblende, potash feldspar. Epidote, apatite, sphene and opaques constitute the accessory minerals (**Figure 5(a)**). Quartz is present as strained grains and includes incipient sub-grains. Plagioclase crystals are idiomorphic or hypidiomorphic, mostly unzoned and poikilitic, moderately altered to sericites and epidotes. The plagioclase is characterized by lamellar, manabech and pericline twins, and the microcline perthite is of stringe perthitic nature. Plagioclase either occurs as large phenocrysts of 300 - 400 μm (**Figure 5(b)**) porphyritic variety and as equigranular grains of 50 - 100 μm. K-feldspar and quartz crystals are mostly allotriomorphic. Hornblende occurs as idiomorphic to hypidiomorphic rhombus with strong pleochroism and intergrown with granular quartz and biotite. Biotite occurs as dark reddish brown to yellowish brown pleochroic crystals in the groundmass.

Monzogranite shows hypidiomorphic texture, composed of subhedral microcline crystals of 300 to 500 μm in equigranular variety and 2 - 3 mms crystals in porphyritic variety (**Figure 5(c)**, **Figure 5(d)**), sericitised plagioclase and allotriomorphic quartz. Chloritised biotite crystals occur as trace minerals. Exsolution and intergrowth textures like perthitic and granophyric are very common. These granites show microstructural deformation features, viz., strained quartz grains, kinked mica and deformation twins in plagioclase.

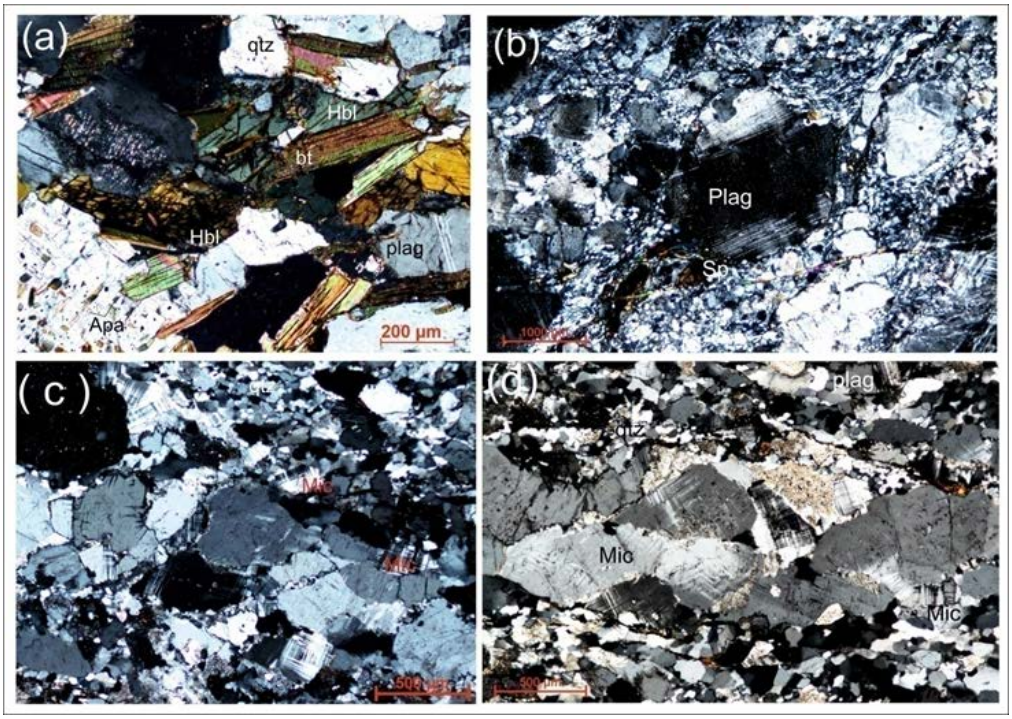

Figure 5. (a) Equigranular granodiorite with hypidiomorphic plagioclase and hornblende and allotriomorphic quartz and biotite. Apatite occurs as acicular crystals; (b) Plagioclase phenocryst in a groundmass of quartz, microcline and plagioclase; (c) Equigranular microcline crystals in monzogranites; (d) Phenocryst of microcline in fine groundmass of recrystallized quartz and sericitized plagioclase. Qtz: quartz; bt: biotite; Hbl: hornblende; Apa: apatite; Sp: sphene; Mic: microcline.

5. Analytical Methods

24 samples of granitoids have been studied as part of whole rock geochemistry. 04 nos of samples of migmatite gneiss, 08 nos of granodiorite samples and 12 nos of monzogranite samples are chemically analyzed along with their C.I.P.W. norm values (Table 1). Major oxide geochemistry of the granitoids was carried out in Chemical Division of Geological Survey of India, Southern Region, Hyderabad. Fresh, unaltered samples of 1 - 1.5 kgs weight were collected from each of the granitoids observed in the area. The samples were, then, crushed and pulverized to −120 micron size for chemical analysis. Major oxide data have been provided by X-Ray Fluorescence (XRF) instrument PANalyticalmagix 2424 (WD XRF) of power 2.4 kw at Chemical Division of Geological Survey of India, Southern Region, Hyderabad. Samples are prepared using the pressed pellet method. To ensure precision of data, the instrument is calibrated with 7 international standards (4 inhouse standards).

Table 1. Whole rock geochemistry of granitoid samples of study area.

Sample Id	PCS-12	PCS-13	PCS-20	PCS-14	BRS-30	BRS-31	BRS-45	BRS-40	PCS-2	PCS-11	PCS-17	BRS-92
Lithology	**Monzogranite**											
SiO_2	76.37	70.3	73.73	73.2	75.61	72.61	77.54	82.09	74.2	73.83	73.35	73.6
Al_2O_3	12.9	15.19	13	14.43	12.29	14.23	13.03	9.39	12.89	13.54	12.64	13.93
FeOt	1.01	2.07	1.54	1.36	0.89	2.47	1.7	0.74	0.85	1.2	2.09	1.62
MnO	0.01	0.04	0.03	0.02	0.02	0.06	0.03	0.01	0.02	0.05	0.04	0.03
MgO	0.21	0.33	0.21	0.15	0.12	0.46	0.19	0.18	0.12	0.13	0.3	0.14
CaO	0.16	1.67	1.25	0.73	0.54	1.26	0.19	0.25	0.99	0.65	0.97	0.51
Na_2O	4.28	4.6	3.8	4.47	3.45	4.21	2.87	2.58	3.87	3.44	3.95	3.85
K_2O	4.35	4.24	4.53	4.78	4.82	3.03	4.12	3.23	4.58	5.17	4.54	5.31
TiO_2	0.07	0.24	0.16	0.1	0.1	0.31	0.1	0.07	0.04	0.12	0.28	0.17
P_2O_5	0.05	0.1	0.06	0.04	0.03	0.1	0.03	0.03	0.02	0.05	0.12	0.07
Trace Elements												
Ba	363.76	1794.41	776.62	885.21	221.54	757.54	496.87	353.34	188.43	646	709.36	1230.48
Ga	15.028	16.059	14.763	15.614	17.889	18.606	15.766	11.613	24.577	15	15.628	17.264
Sc	1.75	5.28	1.75	1.75	<3.5	5.55	<3.5	<3.5	1.75	1.75	1.75	<3.5
V	10	23.84	10	10	<20	25.33	<20	<20	10	10	10	<20
Th	27.9	21.86	31.14	30.19	23.67	16.54	23.03	20.28	35.92	23	46.44	36.82
Pb	9.83	19.66	20.74	26.09	31.28	12.57	18.47	24.29	60.45	22	29.42	30.03
Ni	2.11	8.25	1	3.87	<2	10.39	<2	<2	1	1	3.63	3
Co	1.26	4.32	5.11	2	5.42	5.3	2.65	3.75	1.4	3	4.56	2.7
Rb	180.01	143.83	151.14	157.7	206.89	88.89	119.79	89.64	208.38	161	174.67	161.22
Sr	44.17	231.6	129.08	86.25	62.72	188.51	78.55	40.7	69.18	75	181.23	149.65

Continued

Y	22.96	10.68	13.72	13.5	11.48	25.79	11.77	6.29	22.17	16	33.71	20.41
Zr	85.33	113.77	120.99	135.86	92.47	176.48	90.08	60.6	152.46	86	245.2	212.1
Nb	12.06	6.78	7.17	9.33	9.37	13.23	9.46	2.5	26.07	8	26.95	11.96
Cr	7.5	7.5	7.5	7.5	<15	<15	<15	<15	22.45	7.5	7.5	<15
Cu	0.5	8.51	2.08	3.48	<1	<1	<1	2.64	10.22	2	4.08	1.96
Zn	0.5	82.6	68.68	40.34	21.42	218.59	36.35	34.68	18.86	53	62.87	229.8
Mo	10.12	5.68	4.29	4.89	0.95	0.92	<0.3	3.14	2.59	1.39	4.97	1.18
Sn	2.50	2.50	2.50	2.50	<5	5.41	<5	<5	2.50	16.91	2.50	<5
La	22.03	60.08	7.22	25.41	12.29	49.78	9.90	25.11	12.84	37.68	64.53	9.06
Ce	43.39	98.54	12.19	59.29	21.04	63.52	41.77	47.67	21.64	68.53	115.41	25.43
Pr	5.52	9.99	1.17	5.55	2.65	9.28	2.71	4.82	2.74	8.54	12.69	2.60
Nd	19.19	31.64	4.85	19.82	8.99	32.21	9.55	15.42	9.53	25.36	43.21	9.89
Eu	0.40	0.86	0.17	0.57	0.41	1.09	0.52	0.43	0.36	0.55	1.11	0.30
Sm	4.21	3.87	0.85	3.83	1.68	5.76	2.09	2.35	1.94	3.83	7.57	3.26
Tb	0.56	0.31	0.19	0.44	0.21	0.79	0.26	0.20	0.34	0.37	0.98	0.93
Gd	3.43	2.25	0.93	2.70	1.40	4.98	1.68	1.48	1.80	2.51	5.75	4.55
Dy	3.07	1.63	1.28	1.95	1.29	4.30	1.70	0.91	2.16	1.75	5.37	6.14
Ho	0.59	0.27	0.24	0.35	0.26	0.78	0.35	0.17	0.48	0.32	1.03	1.24
Er	1.92	0.78	0.78	1.03	0.87	2.21	0.99	0.47	1.85	1.05	3.34	3.73
Tm	0.33	0.15	0.12	0.15	0.16	0.36	0.20	0.08	0.40	0.16	0.55	0.57
Yb	2.16	1.01	0.81	1.00	1.09	2.18	1.32	0.54	3.38	0.95	3.41	3.67
Lu	0.35	0.18	0.12	0.18	0.18	0.34	0.23	0.09	0.72	0.15	0.54	0.52
W	2.5	2.5	2.5	2.5	<5	<5	7.11	68.91	2.5	2.5	2.5	<5
Rb/Sr	4.08	0.62	1.17	1.83	3.30	0.47	1.53	2.20	3.01	2.15	0.96	1.08
Eu/Eu*	0.32	0.89	0.58	0.54	0.82	0.62	0.85	0.70	0.59	0.54	0.51	0.24
LaN/LuN	6.54	34.67	6.25	14.66	7.09	15.21	4.47	28.98	1.85	26.09	12.41	1.81
CIA	51.79	50.11	49.27	51.07	50.90	53.39	57.82	53.46	49.58	52.19	49.12	51.81
CIPW												
Q	34.32	23.54	31.64	27.24	35.85	33.43	44.48	54.01	32.03	32.60	30.97	29.79
C	0.98	0.24	0.00	0.67	0.49	1.97	3.58	1.27	0.00	1.22	0.00	1.09
Or	25.71	25.06	26.77	28.25	28.48	17.91	24.35	19.09	27.07	30.55	26.83	31.38
Ab	36.22	38.92	32.15	37.82	29.19	35.62	24.29	21.83	32.75	29.11	33.42	32.58
An	0.47	7.63	5.03	3.36	2.48	5.60	0.75	1.04	4.27	2.90	3.35	2.07
Di	0.00	0.00	0.26	0.00	0.00	0.00	0.00	0.00	0.35	0.00	0.00	0.00
Wo	0.00	0.00	0.00	0.00	0.00	0.00	0.00	0.00	0.00	0.00	0.00	0.00
Hy	0.52	0.82	0.40	0.37	0.30	1.15	0.47	0.45	0.14	0.32	0.75	0.35

Continued

Ol	0.00	0.00	0.00	0.00	0.00	0.00	0.00	0.00	0.00	0.00	0.00	0.00
Il	0.02	0.09	0.06	0.04	0.04	0.13	0.06	0.02	0.04	0.11	0.09	0.06
Tn	0.00	0.00	0.31	0.00	0.00	0.00	0.00	0.00	0.04	0.00	0.48	0.00
Ru	0.06	0.20	0.00	0.08	0.08	0.24	0.07	0.06	0.00	0.06	0.04	0.14
Ap	0.12	0.24	0.14	0.09	0.07	0.24	0.07	0.07	0.05	0.12	0.28	0.17
Sum	98.41	96.72	96.78	97.93	96.99	96.28	98.11	97.84	96.74	96.99	96.21	97.62
Sample Id	**PCS-6**	**BRS-29**	**BRS-19**	**BRS-20**	**PCS-15**	**PCS-19**	**BRS-34**	**BRS-35**	**PCS-16**	**BRS-41**	**BRS-51**	**BRS-52**
Lithology				**Granodiorite**						**Migmatite gneiss**		
SiO_2	59.99	63.57	65.02	47.66	66.25	62.12	67.58	66.38	64.08	56.62	74.38	72.11
Al_2O_3	13.9	15.16	12.94	17.12	14.64	13.29	14.67	15.09	14.96	12.68	13.43	14.28
FeOt	7.9	7.56	6.58	11.52	4.46	7.43	5.06	5.03	6.13	10.02	1.06	1.15
MnO	0.11	0.12	0.08	0.11	0.06	0.09	0.09	0.08	0.09	0.1	0.02	0.02
MgO	3.02	3.35	1.39	4.98	1.37	2.42	1.19	0.79	2.41	4.53	0.22	0.16
CaO	4.99	2.72	3.3	7.26	4.28	5.43	2.75	3.16	4.14	5.69	1.2	1.38
Na_2O	2.85	2.51	3.61	3.21	4.23	3.87	3.25	2.56	3.7	3.25	3.91	3.66
K_2O	2.44	2.26	3.23	3.36	2.78	2.39	2.77	3.52	2.12	2.36	3.73	4.89
TiO_2	0.71	0.83	1.12	1.34	0.49	1.19	0.61	0.39	0.45	1.28	0.06	0.09
P_2O_5	0.28	0.44	0.38	0.95	0.21	0.37	0.21	0.15	0.1	0.89	0.03	0.04
Trace Elements												
Ba	647.27	416.33	767.89	2316.03	2073.62	1131.27	1362.71	1354.05	534.06	965.04	825.67	714.19
Ga	20.941	20.599	21.472	18.146	17.199	19.774	18.09	17.932	19.111	19.653	14.578	17.914
Sc	16.31	12.49	10.59	18.77	10.46	15.69	10.06	9.62	14.25	15.66	<3.5	<3.5
V	142.55	98.17	40.34	220.68	72.84	81.84	62.02	65.64	118.21	131.25	<20	<20
Th	4.94	15.05	15.45	<4	15.2	10.76	16.27	16.66	6.71	8.77	6.52	12.54
Pb	14.55	26.64	18.7	17.17	11.84	14.87	14.97	20.21	11.3	18.64	16.77	18.68
Ni	35.73	35.8	18.07	28.69	18.38	34.55	10.56	7.43	38.88	42.78	<2	2.95
Co	13.76	12.82	14.26	31.8	6.69	20.87	9.69	3.2	19.78	26.41	<1	2.11
Rb	96	122.44	105.2	79.76	56.69	49.76	84.49	123.43	68.84	66.35	66.69	104.99
Sr	383.35	298.43	290.61	2308.53	434.08	368.22	263.52	197.64	298.09	734.25	222.81	222.98
Y	21.01	34.47	50.39	28.61	19.64	29.5	19.63	16.42	15.19	28.24	8.37	8.73
Zr	165.76	258.07	386.29	160.32	220.64	316.9	214.42	148.14	118.5	362.14	70.96	83.4
Nb	8.11	20.22	39.39	9.04	8.13	22.95	13.53	10.07	5.08	20.47	2.5	5.02
Cr	53.27	45.79	35.3	<15	7.5	29.89	17.21	<15	51.93	60.94	<15	<15
Cu	19.74	8.18	17.74	42.96	22.14	33.86	15.13	13.49	40.15	46.52	4.45	<1
Zn	119.76	116.97	102.04	121.26	114.83	102.4	252.61	83.54	181.9	148.93	80.38	70.07
Mo	0.15	1.84	1.18	0.45	3.83	3.92	<0.3	<0.3	3.53	2.03	1.15	<0.3

Continued

Sn	2.50	6.40	<5	<5	2.50	2.50	9.86	<5	2.50	<5	<5	<5
La	27.66	73.83	84.40	94.22	84.87	77.06	80.77	53.19	14.43	133.24	8.71	7.79
Ce	56.19	157.98	184.90	208.33	151.33	136.60	198.51	89.32	26.41	241.54	13.99	12.75
Pr	7.78	17.65	20.37	23.93	16.88	15.71	15.41	9.83	3.15	26.01	1.76	1.55
Nd	31.28	66.21	77.67	96.51	59.05	57.52	52.26	32.52	13.09	96.16	6.63	5.80
Eu	1.46	2.35	2.80	5.24	1.84	2.65	1.68	1.00	0.74	3.54	0.48	0.43
Sm	5.47	11.79	14.77	16.27	8.75	9.78	7.64	4.86	2.59	14.63	1.57	1.51
Tb	0.60	1.31	1.89	1.37	0.89	1.23	0.81	0.48	0.39	1.33	0.24	0.19
Gd	4.27	8.88	12.53	11.35	5.51	7.89	5.50	3.50	2.38	10.12	1.41	1.12
Dy	3.44	6.54	10.15	6.25	4.18	5.79	4.13	2.62	2.34	6.20	1.33	0.88
Ho	0.61	1.12	1.84	0.96	0.78	1.07	0.71	0.46	0.45	0.99	0.27	0.17
Er	1.76	3.14	5.11	2.37	2.32	3.05	2.06	1.34	1.37	2.55	0.61	0.46
Tm	0.25	0.47	0.79	0.34	0.35	0.44	0.32	0.22	0.21	0.35	0.12	0.08
Yb	1.69	2.79	4.57	1.74	2.54	2.66	1.82	1.37	1.18	2.07	0.79	0.47
Lu	0.27	0.44	0.69	0.26	0.38	0.45	0.29	0.20	0.19	0.30	0.11	0.08
W	6.04	<5	<5	<5	2.5	2.5	5.24	<5	2.5	<5	38.35	<5
Rb/Sr	0.25	0.41	0.36	0.03	0.13	0.14	0.32	0.62	0.23	0.09	0.30	0.47
Eu/Eu*	0.92	0.70	0.63	1.18	0.81	0.92	0.79	0.74	0.91	0.89	0.99	1.01
LaN/LuN	10.64	17.43	12.71	37.64	23.20	17.79	28.93	27.62	7.89	46.13	8.22	10.11
CIA	53.63	58.61	46.05	54.66	46.38	46.45	52.65	55.23	50.83	48.90	51.53	50.86
CIPW												
Q	20.75	30.75	24.53	0.00	21.93	19.01	31.01	30.50	22.69	14.28	34.55	29.03
C	0.00	4.69	0.00	0.00	0.00	0.00	1.83	1.68	0.00	0.00	0.85	0.55
Or	14.42	13.36	19.09	19.86	16.43	14.12	16.37	20.80	12.53	13.95	22.04	28.90
Ab	24.12	21.24	30.55	27.16	35.79	32.75	27.50	21.66	31.31	27.50	33.09	30.97
An	17.93	10.62	9.56	22.38	12.75	11.83	12.27	14.70	17.95	13.04	5.76	6.59
Di	2.30	0.00	0.57	2.49	4.39	6.93	0.00	0.00	0.56	4.13	0.00	0.00
Wo	0.00	0.00	0.00	0.00	0.00	0.00	0.00	0.00	0.00	0.00	0.00	0.00
Hy	6.46	8.35	3.20	2.69	1.38	2.82	2.96	1.97	5.74	9.37	0.55	0.40
Ol	0.00	0.00	0.00	6.00	0.00	0.00	0.00	0.00	0.00	0.00	0.00	0.00
Il	0.24	0.26	0.17	0.24	0.13	0.19	0.19	0.17	0.19	0.21	0.04	0.04
Tn	1.44	0.00	2.53	2.99	1.04	2.67	0.00	0.00	0.86	2.87	0.00	0.00
Ru	0.00	0.70	0.00	0.00	0.00	0.00	0.51	0.30	0.00	0.00	0.04	0.07
Ap	0.66	1.04	0.90	2.25	0.50	0.88	0.50	0.36	0.24	2.11	0.07	0.09
Sum	88.31	90.99	91.10	86.05	94.33	91.20	93.14	92.14	92.06	87.46	96.99	96.64

Mineral chemistry of the constituent mineral phases was determined by Electron ProbeMicro Analysis, EPMA SX100 of Cameca (France), with 5 vertically mounted Wavelength Dispersive Spectrometers for WDS analysis and LAB6 crystal, make installed Regional Petrological Laboratory of GSI, SR, Hyderabad is used for EPMA studies. Operating conditions of 15 keV accelerating voltage and 15 nA of beam current was used for major elements. A counting time of 10 seconds was used. For Xray measurements diffracting crystals like PET, TAP and LIF crystals were used depending on the measured elements. Beam diameter was set to 1 micron. Well known and internationally accepted standards developed by P&H Developers were used for calibration. Analytical uncertainty (standard deviation) during the calibrations and analysis of samples was <1%. During the analysis of silicate phases, K alpha lines were used for measurement for analysis of major elements like Si, Ti, Al, Cr, Mn, Fe, Ni, Mg K, Ca, Na and P.

6. Whole Rock Geochemistry

All samples of granitoids of the study area are unaltered and fresh with CIA values varying from 49.12 to 57.82 for monzogranites, 46.05 to 58.61 for granodiorites and 48.9 to 51.53 for migmatite gneiss (**Table 1**). From the biplot of clr-transformed data of each sample, it is observed that the samples of monzogranite, granodiorite and migmatite gneiss trend perpendicular to the PC1 coordinate, which indicates all of them to be unweathered igneous rocks (**Figure 6(a)**). All the samples plot near the igneous rock trend line in the MFW ternary plot and away from the W index, indicting the samples to be fresh and unweathered (**Figure 6(b)**; calculations as per [20]). All the samples have normative quartz and hypersthenes.

In the normative QAP classification diagram (**Figure 7(a)**), all the samples of monzogranites, plot in the monzogranite field while all the samples of granodiorite and migmatite gneiss falls either in the granodiorite field or near it. On the Ab–An–Or diagram [21], the samples plot within the expected fields (**Figure 7(b)**). Samples of migmatite gneiss are taken from both leucosome and melanosome part. It is observed that the samples of leucosome fall in the granite field and those of melanosome fall in the granodiorite field. The TAS classification of the granitoids follow similar trend wherein the monzogranite samples occupy the granite to monzogranite field and the granodiorite samples span from granodiorite to diorite (**Figure 7(c)**). All the samples plot in the sub alkaline field, defined by [22]. On the other hand, in the R1-R2 plot, monzogranite samples plot in the granite to alkali granite field and granodiorite samples plot in the granodiorite to tonalite field (**Figure 7(d)**). The samples of the granitoids are then plotted on a series of discrimination plots to identify and genetically classify the granites (**Figure 8**; after [23]). Based on the plots, it is observed that majority of the granitoids plot in the I- & S-type field. A few samples that though falls on the line separating the two fields, is not consistent in every diagram. All the samples are metaluminous to peraluminous in the molar $Na_2O + Al_2O_3 + K_2O$ plot (**Figure 9(a)**), however, the samples of monzogranite have lower A/NK ratio than the samples of granodiorite and migmatite gneiss.

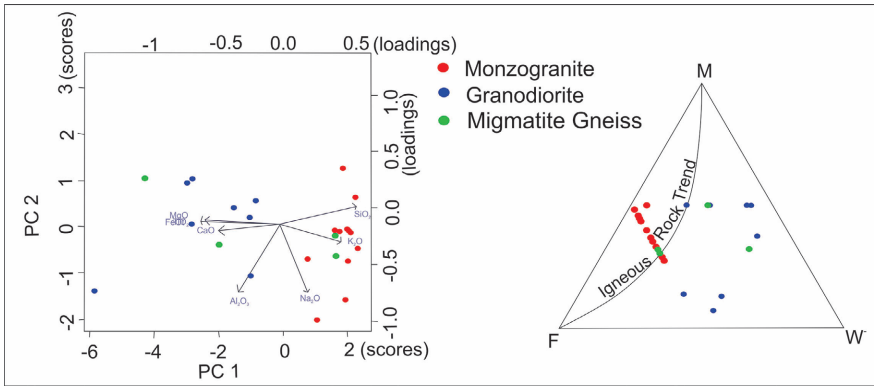

Figure 6. (a) Binary plot of PC1 vs PC2 (Trends of monzogranite, granodiorite and migmatite gneiss is perpendicular to PC1 coordinate, indicating the samples to be unweathered, fresh samples; (b) MFW ternary plot of samples away from W index, indicating fresh samples (after [20]).

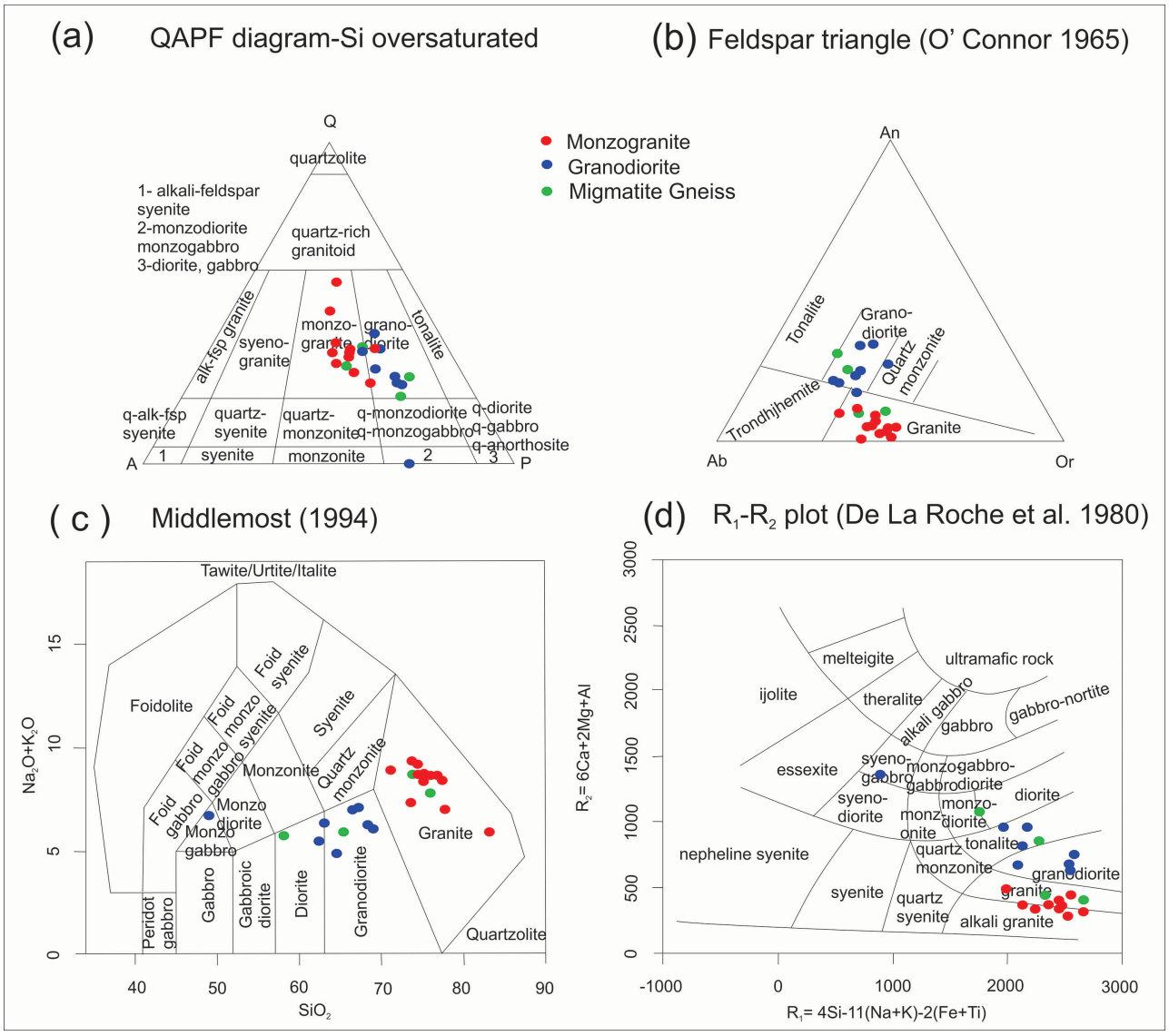

Figure 7. (a) Normative QAP classification diagram; (b) Feldspar Diagram [21]; (c) TAS classification diagram [25]; (d) R1-R2 classification diagram (after [26]) of all the samples of granitoids of the study area.

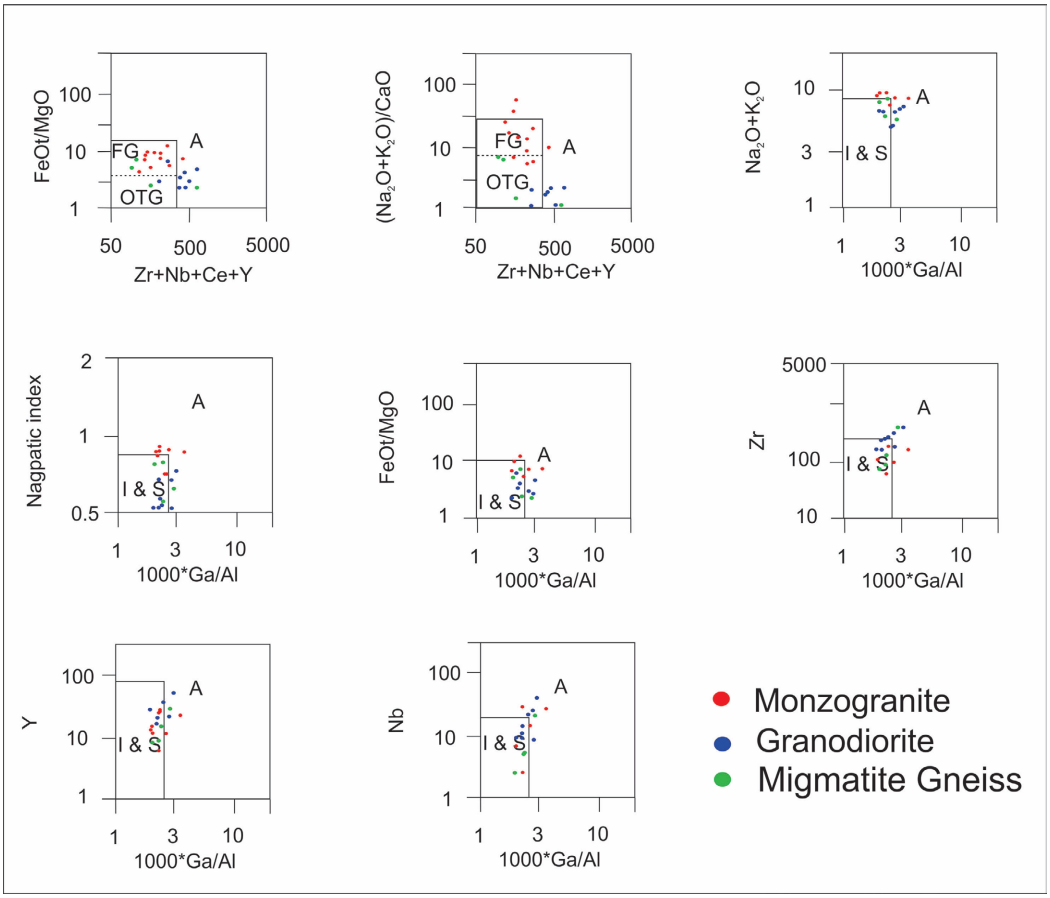

Figure 8. Discrimination plots to distinguish the samples of A-type to I-, S- & M- type. Majority of the samples plot in the I- & S-type (modified after [23]).

In the B-A plot and A/CNK-A/NK plot, the monzogranite samples plot either within or close to the peraluminous field and the granodiorite samples plot in the metaluminous field (**Figure 9(b)**, **Figure 9(d)**). Samples of migmatite gneiss show variable character. The monzogranites samples fall close to the S-Type field than the granodiorite samples in the A/CNK-A/NK plot. The entire samples plot in S-type field in $CaO-Al_2O_3 + Na_2O + K_2O-FeO_t + MgO$ ternary plot but the granodiorite samples have higher CaO content than the monzogranites (**Figure 9(c)**). Presence of hornblende in the granodiorites is also indicative of I-type granite affinity.

The samples plot in the High K-calc-alkaline and shoshonite series in the Co-Th plot (**Figure 10(a)**). On the SiO_2-K_2O plot, the monzogranite samples plot in the high-K calc-alkaline series and granodiorite samples plot in the calc-alkaline to high-K calc-alkaline series (**Figure 10(b)**). In the SiO_2 vs $FeO_t/(FeO_t + MgO)$ plot and SiO_2 vs $Na_2O + K_2O$-CaO plot, the monzogranites plot in the ferroan field and straddle fields of alkali to calc-alkalic, respectively (**Figure 10(c)**, **Figure 10(d)**). The granodiorites and migmatite gneiss are both ferroan and magnesian in nature and occur along the boundary between alkali and alkali-calcic field [24].

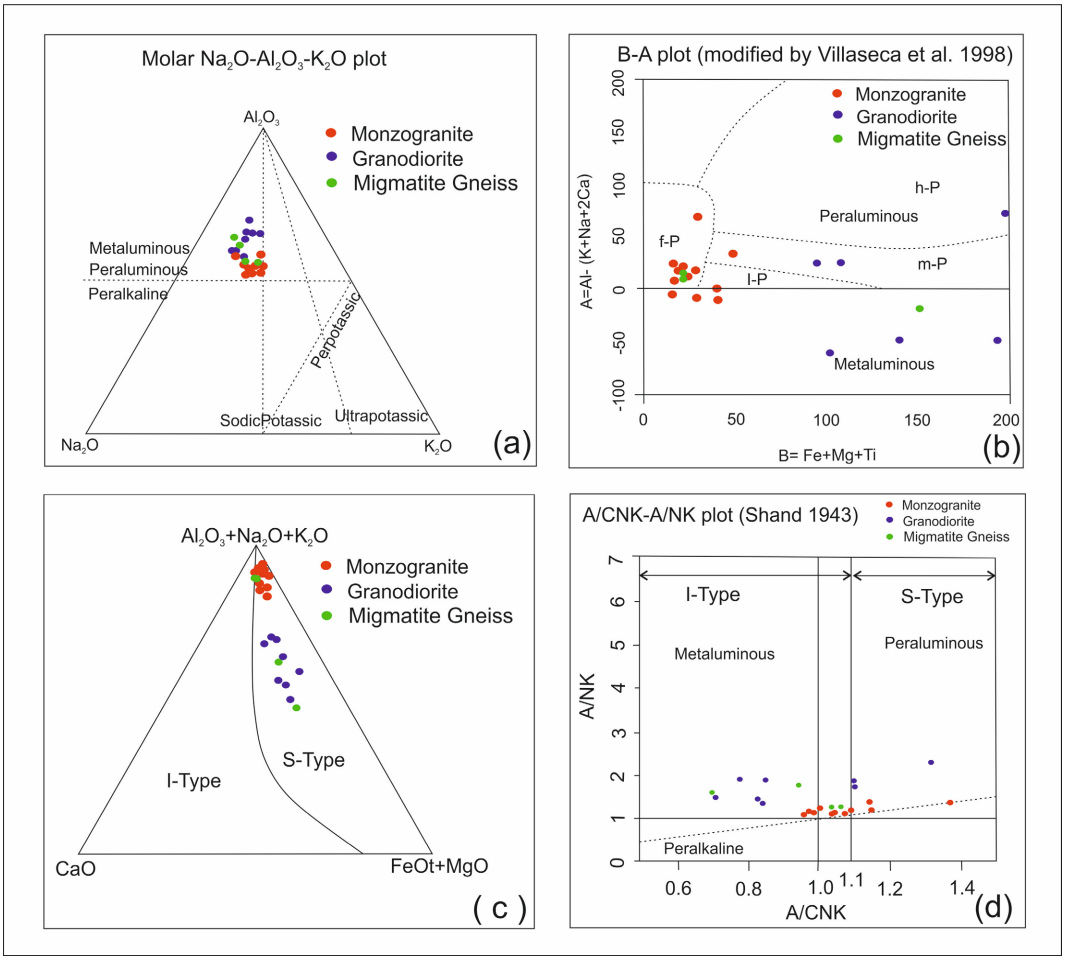

Figure 9. (a) Molar Na_2O-Al_2O_3-K_2O plot; (b) B-A plot (after [27]); (c) CaO-Al_2O_3 + Na_2O + K_2O-FeO_t + MgO plot; (d) A/CNK vs A/NK plot.

On the primitive mantle normalized multi-element spider diagrams, samples of granodiorite show similar patterns with more or less same degree of elemental enrichment. They show characteristic features common to I-type granites, viz., distinctive depletion of LILE's like Ba, and HFSE's like Nb, P and Ti relative to other trace elements (**Figure 11(a)**).

Chondrite normalized REE patterns reveal a distinction between monzogranite and granodiorite (**Figure 11(b)**), where samples of granodiorite show similar patterns with a lesser degree of REE fractionation ($(La/Yb)_N$ =11.03 - 36.51) than monzogranite, which shows a higher degree of fractionation ($(La/Yb)_N$ = 1.66 - 40.10). The granodiorite has high ΣREE (an average 327.905 ppm) content, and shows LREE enrichment ($(La/Sm)_N$ = 3.1 - 6.8) with enriched but relatively flat HREE ($(Gd/Yb)_N$ = 1.75 - 5.26) patterns and weak negative to positive Eu anomaly (Eu/Eu* = 0.62 - 1.18). Monzogranites, on the other hand, has relatively low ΣREE (an average 118.693 ppm) contents and exhibits strongly fractionated REE patterns with highly enriched LREE ($(La/Sm)_N$ =1.74 - 9.76) and depleted HREE ($(Gd/Yb)_N$ = 0.43 - 2.21) patterns having concave upward shape, and show strong negative Eu anomaly (Eu/Eu* = 0.23 - 0.89).

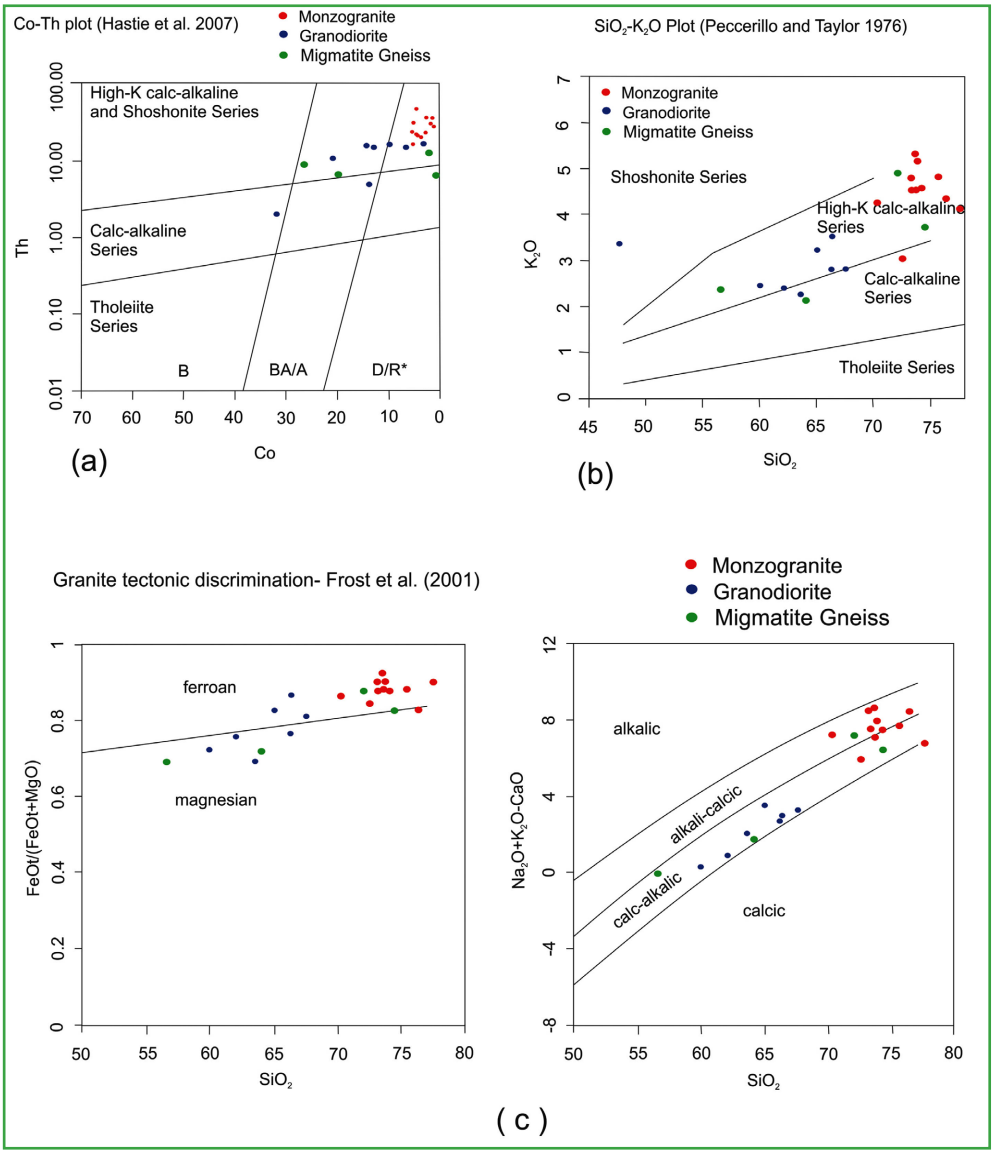

Figure 10. (a) Co-Th plot (after [28]); (b) SiO_2 vs K_2O plot (after [29]); (c) SiO_2 vs $FeO_t/(FeO_t + MgO)$ plot; (d) SiO_2 vs $Na_2O + K_2O$-CaO plot (after 24]).

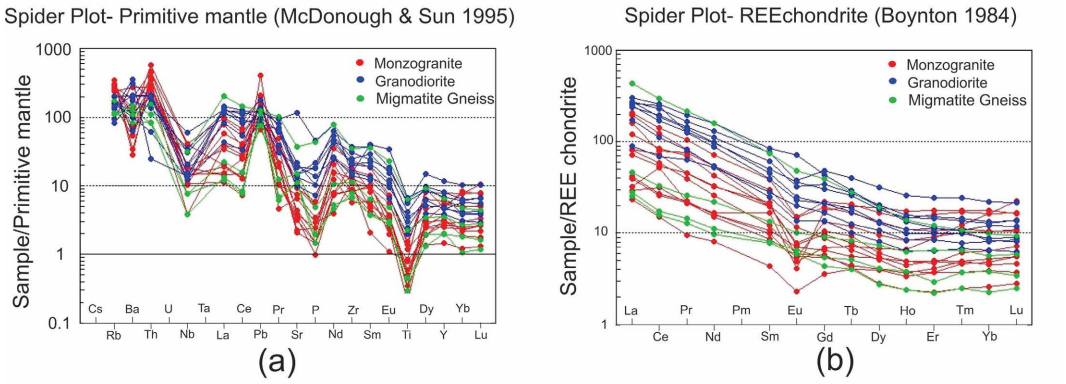

Figure 11. (a) Spider plot of trace elements normalized to primitive mantle (after [30]); (b) Chondrite normalized REE spider plot (after [31]).

Major elements of the granodiorites and migmatite gneiss form well defined clusters and trends in Harker bivariate plots (Figure 12), where TiO_2, P_2O_5, CaO, FeO_t, MgO and MnO concentrations decrease monotonously with increasing amount of SiO_2. K_2O and Al_2O_3 display a weak positive correlation with SiO_2.

In monzogranites, all the oxides except Na_2O show decreasing concentration with respect of SiO_2. Na_2O, however, is independent of the SiO_2 in all the samples. The overall pattern of decreasing TiO_2, FeO_t, MgO and CaO with increasing SiO_2 is characteristic of fractionating granitic systems. The variation patterns of selected trace elements with respect to each other and SiO_2 however indicates fractionation in both monzogranites and granodiorites (Figure 13).

Sr and Zr generally decrease with increasing SiO_2 for all samples of granodiorites and migmatite gneiss whereas Rb and Ba show little correlation with increasing silica. In monzogranites, Ba, Sr and Zr negatively correlate with SiO_2. Rb and Ba are more enriched relative to Sr, and overall Rb/Sr ratios are high but

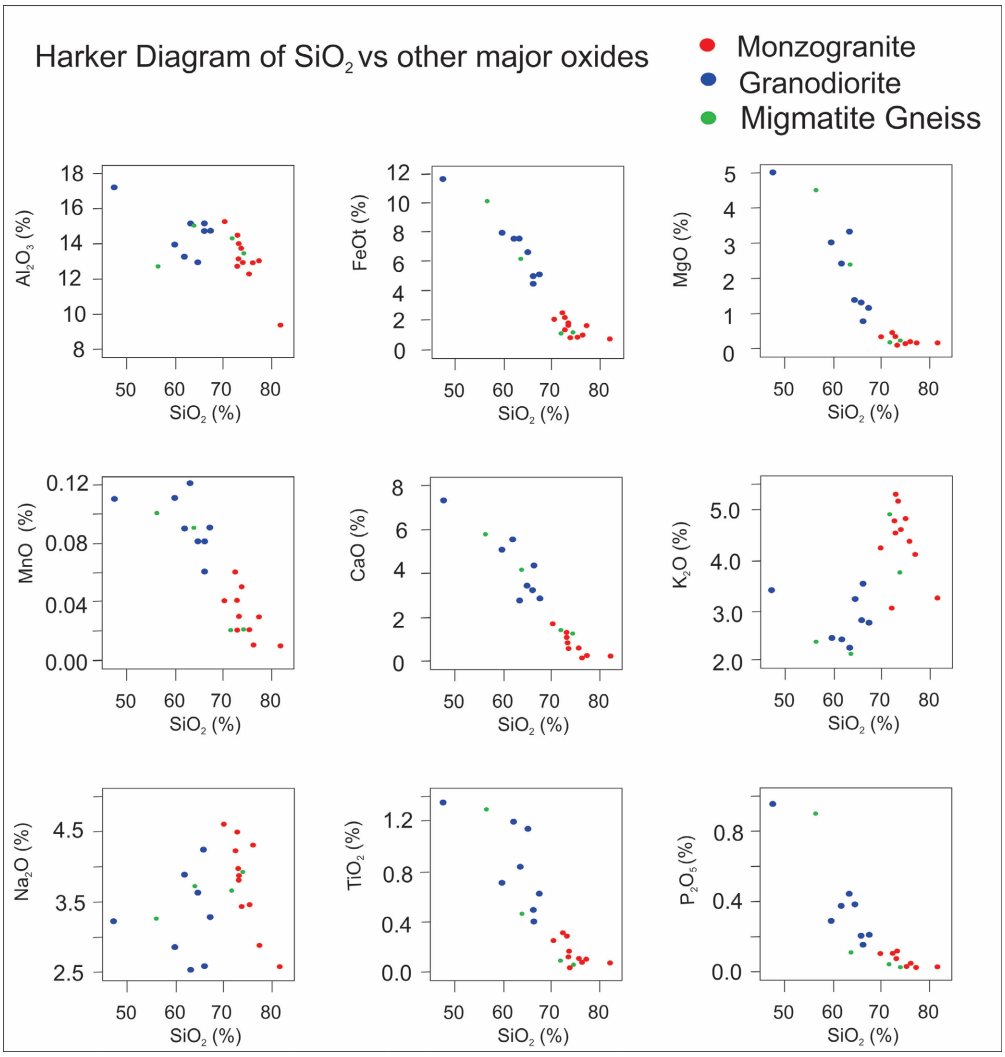

Figure 12. Harker plot of all oxides of granitoid samples of study area with respect to SiO_2.

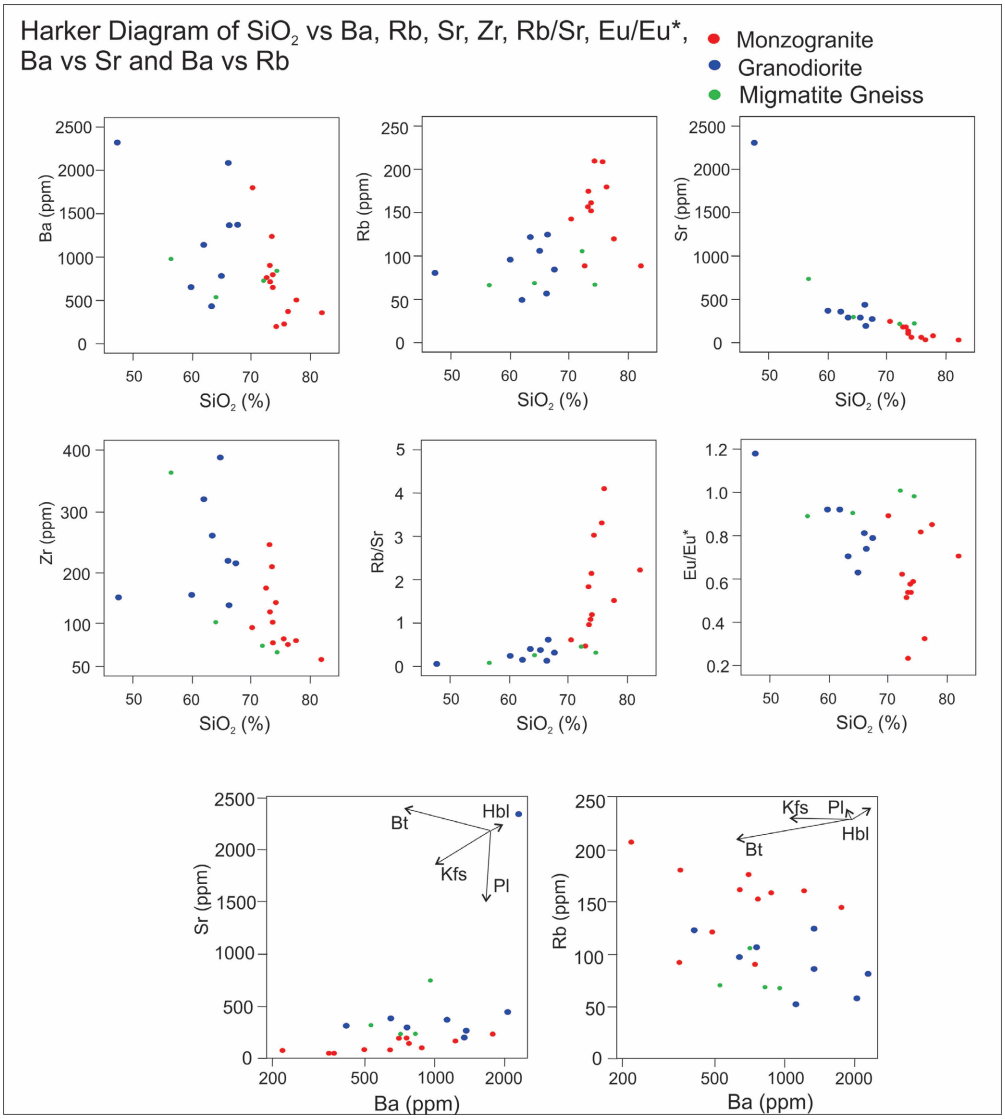

Figure 13. Harker plot of trace elements (Ba, Rb, Sr, Zr, Rb/Sr and Eu/Eu*) of granitoid samples of study area with respect to SiO_2 and binary plots of Ba vs Sr and Ba vs Rb (Partition coefficients for plagioclase (Pl), biotite (Bt), K-feldspar (Kfs) and hornblende (Hbl) are followed from [32]).

comparatively higher in monzogranite (0.62 - 4.08) than granodiorite (0.03 - 0.62). The major and trace elements along with inter-elemental variation diagrams suggest key role of fractional crystallization processes during petrogenesis of these granites, which is more in case of monzogranites. The Ba–Sr plot in logarithmic coordinates shows the presence of two distinct but broadly parallel linear trends, the first represented by monzogranitic and the second by granodioritic samples (**Figure 13(g)**).

The first trend is compatible with up to 15% fractional crystallization of a K-feldspar > plagioclase assemblage. The Ba-Rb plot in lograthmic coordinates confirms that K-feldspar with minor plagioclase fractional crystallization is a plausible model to explain the variation in the monzogranites (**Figure 13(h)**). This is also observed from (Zr + Nb + Ce + Y) vs (K_2O + Na_2O)/CaO plot where

the samples of monzogranites are more fractionated than the granodiorites and thus fall in the fractionated felsic granite field while the granodiorites and migmatite gneiss samples plot in the normal I/S/M-type granites (**Figure 8(b)**). This can be explained by the high K content of the monzogranites.

7. Petrogenesis

On the Granite tectonic discrimination diagram of [33], barring a few, all the granitoids plot in CCG + IAG + CAG field (Group I; **Figures 14(a)-(d)**). Further discrimination within this group I can be accomplished only on the basis of Shand's index (**Figure 9(d)**). Granitoids under CCG usually have A/CNK [$AL_2O_3/(CaO + Na_2O + K_2O)$] values greater than 1.15 [34]. But in the samples of present area, only few samples have values greater than 1.15. Majority of the samples have A/CNK values less than 1.15, which indicates a similar setup of the granitoids in the IAG + CAG group. However, it is not possible to discriminate between IAG and CAG through these diagrams. Accordingly, the most widespread trace-element plot is used to distinguish the tectonic setting of granitoids by the Rb v. (Y + Nb) plot of [35].

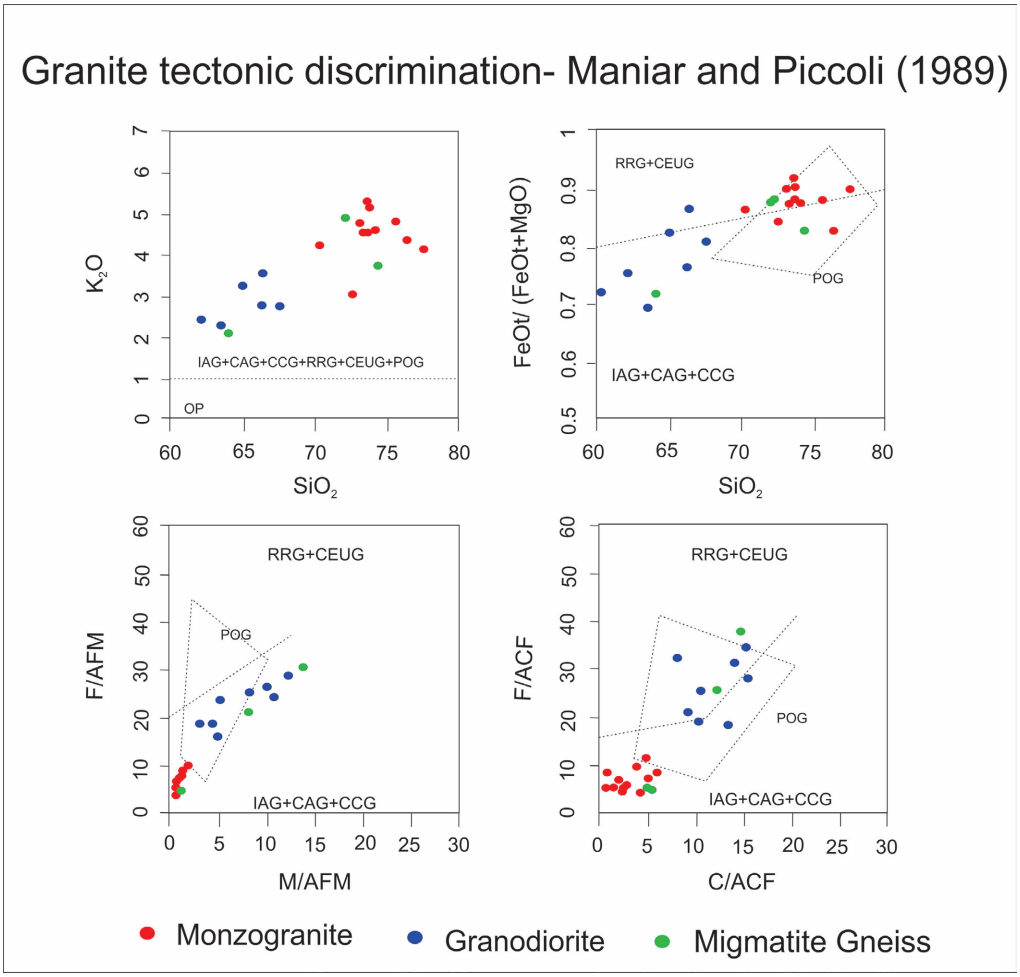

Figure 14. Granite tectonic discrimination diagrams of the granitoid samples (after [19] [33]).

Based on this diagram, the granodiorites and monzogranites plot in the volcanic arc granites (VAG) field (**Figure 15**). According to [35] model (see also [36]), the high Rb component of VAG and/or post-COLG comes from enriched mantle or subducted crust, possibly augmented by Rb-rich, subduction-derived fluids. Incompatible elements, such as Nb + Y are diluted in the melt with higher melting. Hence, their low content in the granodiorites and monzogranites indicate higher melting in these granitoids. The R_1-R_2 scheme of [26], was specifically adapted by [37] into a tectonic framework by modifying the subdivisions postulated by [38]. In this scheme, the granodiorites and migmatite gneiss belong to the pre-plate collision field and the monzogranites straddle the field from post orogenic to syn-collision to Late orogenic fields (**Figure 16**).

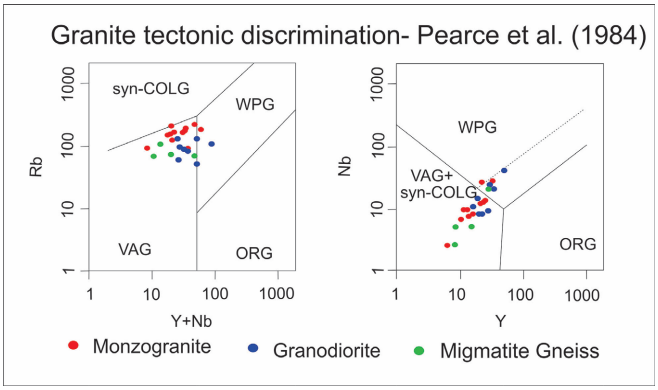

Figure 15. Granite tectonic discrimination diagrams of the granitoid samples (after [35]).

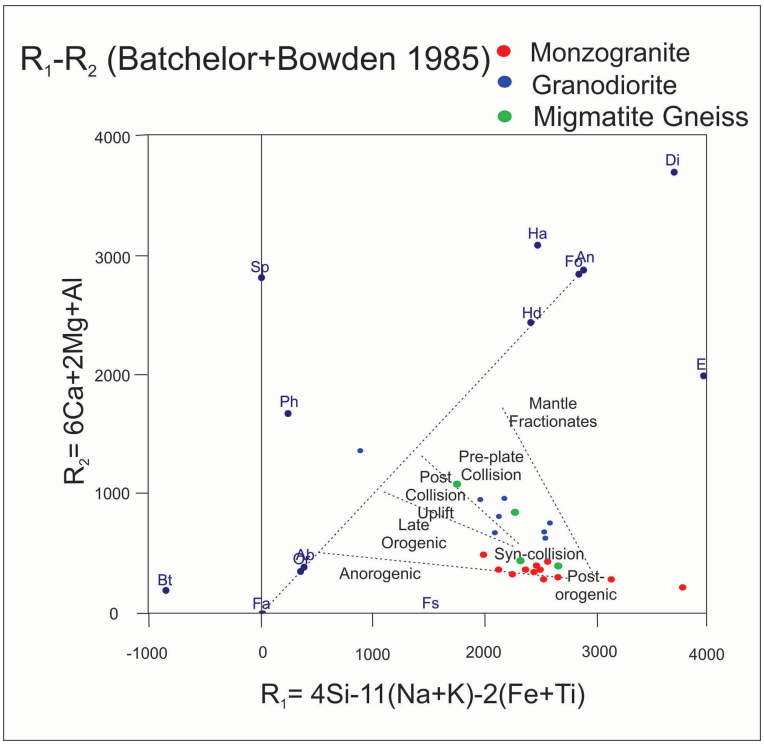

Figure 16. Granite tectonic discrimination (R_1-R_2) diagrams of the granitoid samples (after [37]).

Mineral chemistry of 2 samples of granodiorite and 2 samples of monzogranites are done to determine the dominant mineralogy of the rocks and to determine the emplacement pressure of each (**Figure 17(a)**). The elemental analyses of biotite, hornblende and feldspars are given in **Table 2**, **Table 3**.

Amphibole structural formula was calculated based on 23 oxygen atoms, according to the methods of [39] and [40] and feldspar structural formula are calculated based on 32 oxygen atoms. In the granodiorite samples, feldspars are mostly andesine to oligoclase and amphiboles are tschermakites and edenites (**Figures 17(b)-(d)**). The edenites are mostly observed within the titanite grains or in contact with the same. The monzogranites have dominantly sanidine and some anorthoclase in the rocks, apart from minor albites.

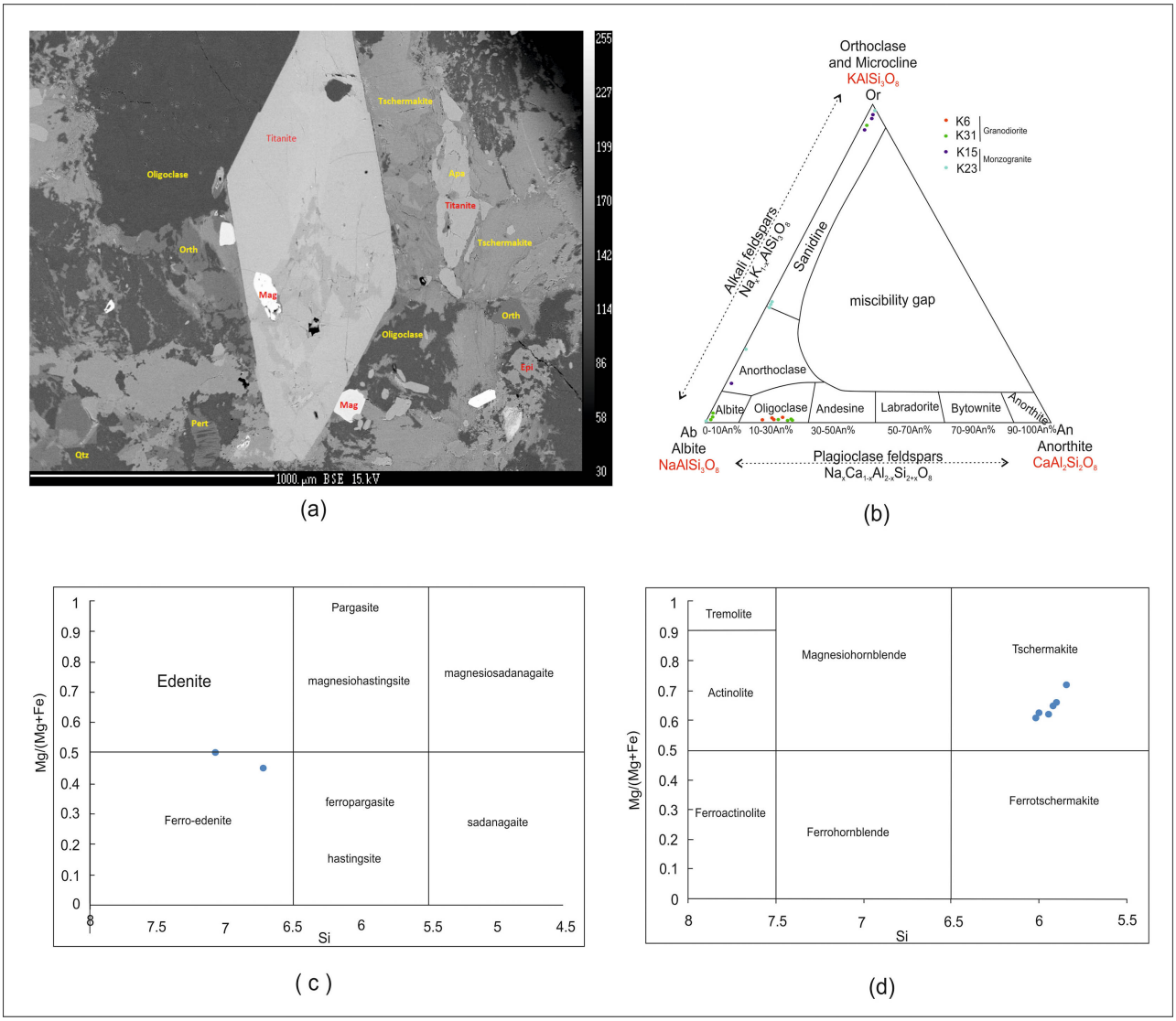

Figure 17. (a) Back scattered image of granodiorite showing the mineral association (Orth-Orthoclase, Pert-Perthite, Apa-Apatitte, Mag-Magnetite, Qtz-Quartz); (b) Triangular plot for feldspar classification; (c) Classification diagram of calcic amphiboles with Na + K of more than 0.5 apfu and Ti of less than 0.5 apfu in their A site; (d) Classification diagram of calcic amphiboles with Na + K of less than 0.5 apfu and Ca of less than 0.5 apfu in their A site.

Table 2. Mineral chemistry of biotite and amphiboles of monzogranite & granodiorite.

	Biotite							Amphiboles							
	Monzogranite				Granodiorite				Granodiorite						
	K15				K31				K6						
DataSet /Point	30/1.	31/1.	33/1.	36/1.	5/1.	6/1.	13/1.	DataSet /Point	5/1.	11/1.	13/1.	15/1.	16/1.	17/1.	18/1.	22/1.
SiO_2	26.515	27.018	26.409	26.007	36.592	37.172	39.465	SiO_2	47.54	37.11	38.15	38.42	37.78	37.25	44.71	37.87
TiO_2	0.012	0.031	0	0.005	2.314	2.11	0.032	TiO_2	0.15	0.88	1.84	1.90	1.72	1.45	0.46	1.74
Al_2O_3	18.712	18.291	19.083	18.431	15.977	16.061	22.854	Al_2O_3	6.92	13.80	14.23	13.88	14.15	14.25	9.23	13.86
FeO	31.07	30.82	31.02	30.66	24.73	24.40	12.17	Cr_2O_3	0.00	0.00	0.00	0.04	0.04	0.00	0.01	0.00
MnO	0.42	0.32	0.51	0.45	0.60	0.45	0.66	FeO_{tot}	18.55	19.45	19.89	19.32	19.26	18.93	20.24	19.11
MgO	11.51	11.85	11.42	11.37	7.22	7.08	0.00	MnO	0.59	0.21	0.22	0.18	0.22	0.27	0.54	0.35
CaO	0.12	0.09	0.08	0.20	0.00	0.00	23.55	MgO	10.63	13.06	11.45	12.02	11.95	12.08	9.28	11.30
Na_2O	0.02	0.00	0.00	0.03	0.10	0.04	0.00	CaO	12.75	0.00	0.00	0.00	0.00	0.00	12.09	0.00
K_2O	0.02	0.07	0.02	0.05	9.47	9.45	0.00	Na_2O	0.97	0.02	0.07	0.06	0.00	0.00	1.50	0.05
P_2O_5	0.00	0.00	0.00	0.00	0.00	0.00	0.20	K_2O	0.65	9.09	9.59	9.24	9.56	9.19	1.25	9.34
Cr_2O_3	0.05	0.00	0.04	0.00	0.00	0.01	0.00	NiO	0.06	0.00	0.00	0.00	0.02	0.00	0.00	0.01
NiO	0.05	0.02	0.04	0.00	0.00	0.00	0.09	P_2O_5	0.09	0.00	0.00	0.00	0.00	0.00	0.08	0.00
Total	88.49	88.51	88.62	87.21	97.01	96.77	99.02	Total	**98.90**	93.62	95.43	95.07	94.69	93.42	99.38	93.62
X	−1229	−2001	−8578	−10298	−12173	−12630	14446	X	**−3703**	−3374	−1359	−4938	−4996	−4715	−6093	−4707
Y	−25815	−26011	−20060	−19036	30835	30401	28834	Y	**25512**	24991	25795	33126	33009	32943	33023	32392
Z	−18	−1	103	134	362	357	575	Z	**470.00**	466.00	478.00	456.00	452.00	459.00	457.00	457.00
Si	4.50	4.56	4.47	4.48	5.63	5.71	5.59	Si	7.08	5.85	5.95	6.00	5.92	5.90	6.73	6.02
Al	3.50	3.44	3.53	3.52	2.37	2.29	2.41	Al	0.92	2.15	2.05	2.00	2.08	2.10	1.27	1.98
Al	0.23	0.20	0.27	0.21	0.53	0.61	1.40	Al	0.30	0.41	0.57	0.56	0.53	0.57	0.36	0.62
Ti	0.00	0.00	0.00	0.00	0.27	0.24	0.00	Fe(iii)	0.00	1.37	0.98	0.84	1.04	1.04	0.00	0.86
Fe(ii)	4.40	4.35	4.39	4.41	3.18	3.13	1.44	Ti	0.02	0.10	0.22	0.22	0.20	0.17	0.05	0.21
Mn	0.06	0.05	0.07	0.07	0.08	0.06	0.08	Cr	0.00	0.00	0.00	0.01	0.00	0.00	0.00	0.00
Mg	2.91	2.98	2.88	2.92	1.66	1.62	0.00	Fe(ii)	2.31	1.19	1.62	1.68	1.48	1.47	2.55	1.68
Ca	0.02	0.02	0.02	0.04	0.00	0.00	3.57	Mn	0.07	0.03	0.03	0.02	0.03	0.04	0.07	0.05
Na	0.01	0.00	0.00	0.01	0.03	0.01	0.00	Mg	2.36	3.07	2.66	2.80	2.79	2.86	2.08	2.68
K	0.00	0.02	0.00	0.01	1.86	1.85	0.00	Ca	2.03	0.00	0.00	0.00	0.00	0.00	1.95	0.00
Cl	0.00	0.00	0.00	0.00	0.00	0.00	0.00	Na	0.28	0.00	0.02	0.02	0.00	0.00	0.44	0.02
F	0.00	0.00	0.00	0.00	0.00	0.00	0.00	K	0.12	1.83	1.91	1.84	1.91	1.86	0.24	1.89
TOTAL	15.64	15.62	15.63	15.67	15.60	15.53	14.50	TOTAL	15.50	16.00	16.00	16.00	16.00	16.00	15.74	16.00

Table 3. Mineral chemistry of feldspars of granodiorites and monzogranite.

	Granodiorite														
	K6								K31						
DataSet /Point	4/1.	10/1.	12/1.	14/1.	23/1.	24/1.	7/1.	8/1.	10/1.	11/1.	12/1.	14/1.	15/1.	16/1.	17/1.
Na_2O	10.09	8.82	9.38	9.56	8.96	9.39	9.01	0.23	7.91	0.61	8.30	11.42	0.34	11.27	0.36
P_2O_5	0.04	0.00	0.03	0.07	0.04	0.01	0.01	0.00	0.05	0.00	0.03	0.04	0.00	0.00	0.02
K_2O	0.10	0.17	0.17	0.13	0.24	0.10	0.14	15.57	0.06	13.54	0.09	0.16	16.10	0.45	15.98
TiO_2	0.04	0.00	0.02	0.00	0.00	0.00	0.00	0.00	0.00	0.04	0.02	0.00	0.00	0.02	0.01
Cr_2O_3	0.00	0.01	0.04	0.00	0.00	0.01	0.00	0.00	0.00	0.00	0.00	0.04	0.04	0.06	0.00
FeO	0.08	0.08	0.10	0.09	0.09	0.09	0.00	0.00	0.01	0.05	0.00	0.05	0.01	0.00	0.09
NiO	0.00	0.00	0.00	0.00	0.00	0.00	0.00	0.00	0.00	0.00	0.05	0.00	0.00	0.00	0.00
MgO	0.00	0.00	0.00	0.01	0.00	0.00	0.00	0.00	0.02	0.00	0.00	0.00	0.00	0.00	0.00
SiO_2	64.89	64.13	64.17	63.85	63.92	63.71	64.52	66.83	65.29	67.67	64.40	69.46	66.48	69.25	66.10
CaO	3.51	4.12	4.00	4.24	4.43	4.46	4.32	0.00	4.48	0.00	5.01	0.27	0.00	0.23	0.00
MnO	0.07	0.03	0.00	0.00	0.06	0.00	0.04	0.00	0.00	0.00	0.00	0.06	0.08	0.00	0.00
Al_2O_3	21.89	22.76	22.67	22.75	22.66	22.82	21.97	18.03	23.13	18.60	23.32	19.27	17.87	19.10	17.94
Total	100.71	100.11	100.57	100.70	100.39	100.60	100.00	100.65	100.95	100.51	101.22	100.77	100.91	100.38	100.51
X	−3593	−3524	−1644	−934	−4511	−4614	−11,644	−11,336	13,983	14,623	14,035	14,310	14,333	14,301	14,275
Y	24,910	24,947	25,675	25,833	32,041	31,742	30,962	30,871	29,120	29,196	28,463	29,327	29,320	29,341	29,339
Z	471	471	486	491	468	468	362	371	570	578	570	576	577	576	576
Si	11.40	11.30	11.28	11.23	11.27	11.22	11.39	12.17	11.36	12.20	11.23	12.05	12.15	12.06	12.12
Ti	0.00	0.00	0.00	0.00	0.00	0.00	0.00	0.00	0.00	0.01	0.00	0.00	0.00	0.00	0.00
Al	4.53	4.73	4.70	4.72	4.71	4.73	4.57	3.87	4.74	3.95	4.79	3.94	3.85	3.92	3.88
Fe(ii)	0.01	0.01	0.01	0.01	0.01	0.01	0.00	0.00	0.00	0.01	0.00	0.01	0.00	0.00	0.01
Ca	0.66	0.78	0.75	0.80	0.84	0.84	0.82	0.00	0.83	0.00	0.94	0.05	0.00	0.04	0.00
Na	3.44	3.01	3.20	3.26	3.06	3.20	3.08	0.08	2.67	0.21	2.81	3.84	0.12	3.80	0.13
K	0.02	0.04	0.04	0.03	0.05	0.02	0.03	3.62	0.01	3.11	0.02	0.04	3.75	0.10	3.74
TOTAL	20.06	19.86	19.98	20.05	19.94	20.03	19.89	19.74	19.61	19.49	19.79	19.92	19.87	19.93	19.88
An	16.04	20.31	18.89	19.52	21.17	20.69	20.76	0.00	23.74	0.00	24.89	1.26	0.00	1.07	0.00
Ab	83.39	78.68	80.15	79.75	77.47	78.74	78.42	2.16	75.88	6.42	74.59	97.84	3.11	96.38	3.35
Or	0.57	1.01	0.96	0.73	1.36	0.57	0.81	97.84	0.38	93.58	0.53	0.90	96.89	2.56	96.65

	Monzogranite												
	K15							K23					
DataSet/ Point	29/1.	32/1.	34/1.	37/1.	38/1	39/1.	40/1.	1/1.	7/1.	8/1.	9/1.	10/1.	11/1.
Na_2O	0.39	0.38	0.82	0.17	10.04	0.35	0.32	7.52	7.10	11.98	0.17	0.18	9.40
P_2O_5	0.00	0.00	0.04	0.01	0.02	0.00	0.00	0.00	0.00	0.00	0.00	0.00	0.00
K_2O	16.21	15.29	15.06	15.85	2.15	16.18	16.01	6.59	6.57	0.01	16.24	16.28	4.31
TiO_2	0.00	0.00	0.00	0.00	0.05	0.02	0.07	0.00	0.00	0.00	0.00	0.00	0.00

Continued

Cr_2O_3	0.00	2.87	0.00	0.00	0.10	0.00	0.00	0.00	0.00	0.00	0.00	0.28	0.40
FeO	0.01	0.23	0.00	0.22	0.04	0.14	0.00	0.08	0.09	0.00	0.00	0.00	0.05
NiO	0.00	0.00	0.00	0.00	0.00	0.00	0.00	0.04	0.00	0.00	0.08	0.00	0.00
MgO	0.01	0.00	0.00	0.00	0.01	0.00	0.00	0.01	0.00	0.00	0.00	0.01	0.01
SiO_2	65.83	64.32	66.81	65.82	66.84	65.98	66.30	66.05	67.98	68.30	66.23	63.57	66.10
CaO	0.00	0.00	0.00	0.00	0.28	0.00	0.00	0.07	0.13	0.04	0.00	0.00	0.00
MnO	0.03	0.00	0.01	0.00	0.07	0.00	0.01	0.04	0.00	0.00	0.00	0.00	0.03
Al_2O_3	18.07	17.36	18.10	17.86	20.40	18.17	17.86	18.71	18.59	19.15	17.96	18.20	18.75
Total	100.55	100.46	100.83	99.92	100.00	100.84	100.57	99.11	100.46	99.47	100.69	98.52	99.05
X	−1648.00	−1823.00	−9223.00	−10441.00	−10683.00	−9446.00	−9425.00	−7327.00	−6808.00	−6816.00	−8097.00	−8096.00	−8052.00
Y	−25831.00	−25866.00	−20204.00	−18868.00	−18626.00	−18419.00	−18191.00	26884.00	27069.00	28382.00	28572.00	28477.00	28527.00
Z	−2.00	2.00	118.00	139.00	140.00	118.00	118.00	310.00	302.00	304.00	308.00	308.00	304.00
Si	12.08	12.13	12.15	12.13	11.80	12.07	12.14	11.95	12.08	12.00	12.13	11.98	11.93
Ti	0.00	0.00	0.00	0.00	0.01	0.00	0.01	0.00	0.00	0.00	0.00	0.00	0.00
Al	3.91	3.86	3.88	3.88	4.24	3.92	3.85	3.99	3.89	3.97	3.88	4.04	3.99
Fe(ii)	0.00	0.04	0.00	0.03	0.01	0.02	0.00	0.01	0.01	0.00	0.00	0.00	0.01
Ca	0.00	0.00	0.00	0.00	0.05	0.00	0.00	0.01	0.02	0.01	0.00	0.00	0.00
Na	0.14	0.14	0.29	0.06	3.44	0.12	0.11	2.64	2.44	4.08	0.06	0.06	3.29
K	3.80	3.68	3.49	3.73	0.48	3.78	3.74	1.52	1.49	0.00	3.79	3.91	0.99
TOTAL	19.93	19.85	19.81	19.83	20.03	19.92	19.85	20.13	19.94	20.06	19.86	19.99	20.21
An	0.00	0.00	0.00	0.00	1.35	0.00	0.00	0.32	0.61	0.17	0.00	0.00	0.00
Ab	3.55	3.64	7.63	1.61	86.48	3.17	2.93	63.22	61.77	99.79	1.55	1.63	76.84
Or	96.45	96.36	92.37	98.39	12.17	96.83	97.07	36.46	37.62	0.04	98.45	98.37	23.16

Zircon saturation temperatures (T_{Zr}) calculated from bulk rock compositions provides a simple and robust means of estimating magma temperatures [41] [42]. They have established experimentally that the partition coefficient of zircon D_{Zr} zircon melt is a function of the parameter M [(Na + K + 2Ca)/(Al*Si), all in cation fraction] and temperature. Therefore, using this formula, the Zr thermometry yields the temperature at which the granites of study area formed, *i.e.*, an average T_{Zr} (˚C) ~775˚C for monzogranites, ~812.5˚C for granodiorite and ~785˚C for migmatite gneiss (**Figure 18(a)**).

The geobarometry of the granodiorites are attempted through the Al in hornblende barometry. The Al-in-hornblende barometer [43] [44] [45] [46] [47] [48] is controlled by the total Al-content of hornblende. The intensive parameters pressure, temperature, oxygen fugacity, as well as the whole rock composition and the coexisting phases determine the Al-content of hornblende. Based on these calibrations the pressure calculated for the hornblendes in the granodiorite of the present area can be summarized as in **Table 4**.

Table 4. Calculated pressure in kbar from Al in hornblende with different calibrations.

	Type of hornblende [32]	Al^{tot}	[43]	[44]	[45]	[47]	[48]
5/1	Edenite	1.214176	2.18642	2.08696	1.67522	2.76864	2.368
11/1	Tschermakite	2.561417	8.96183	9.68404	7.37303	9.18036	7.874
13/1	Tschermakite	2.615669	9.23848	9.99424	7.60568	9.44216	8.175
15/1	Tschermakite	2.556932	8.94171	9.66148	7.35611	9.16132	7.852
16/1	Tschermakite	2.613126	9.22339	9.97732	7.59299	9.42788	8.158
17/1	Tschermakite	2.661505	9.46986	10.25368	7.80026	9.66112	8.432
18/1	Edenite	1.636676	4.31411	4.47268	3.46451	4.78212	3.708
22/1	Tschermakite	2.596025	9.14794	9.89272	7.52954	9.35648	8.076

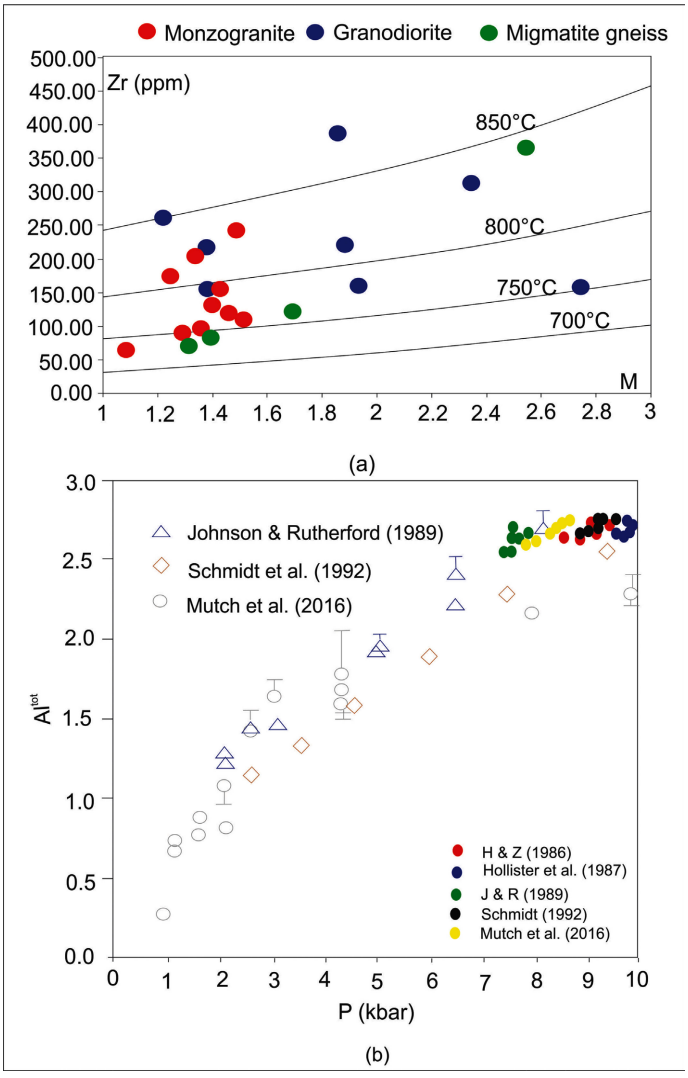

Figure 18. (a) M vs Zr plot for all the granitoid samples of study area showing their crystallization temperature (b) P(kbar) vs Al_{tot} plot of the amphibole sample points of granodiorite to estimate their emplacement pressure.

The granodiorites are I-type in character with some S-type contributions. Calcic amphiboles are typical for I-type intrusives (**Figure 17(c)**, **Figure 17(d)**) [49]. According to [50] magmatic amphiboles contain less than 7.3 apfu of Si atoms, and amphiboles containing more than 7.3 apfu of Si atoms are derived via the subsolidus process [51]. All the amphiboles of granodiorites have Si atoms less than 7.3 apfu however; the edenites do not coexist with plagioclases (they are probably derived from magma that initially crystallized at a considerable depth). Hence, the tschermakites are considered for geobarometry.

Aiming to estimate the pressure, amphibole compositions of the granodiorites of present area were plotted in the diagram P (kbar) × Al_{tot} (**Figure 18(b)**; based on all the calibrated values). The experimental data of [45] [47] and [48] are also shown. It is observed that the compositions of the tschermakites of granodiorites are more compatible with the experimental data of [45] and [48]. However, the geobarometer on calibration of [48] is applicable in a large variety of granitoid rocks containing the mineral assemblage amphibole + plagioclase ($An_{15\text{-}80}$) + biotite + alkali feldspar + quartz + magnetite + ilmenite/titanite + apatite. Such mineral association is found in the granodiorites of present area. Since, the granodiorites are emplaced at same tectonic level and no evidence of tectonic displacement is observed, hence it can be concluded that the emplacement pressure is about 7.85 [±0.6 kbar] to 8.43 [±0.6 kbar] kbar (avg. 8.14 ± 0.6 kbar).

Due to lack of significant geobarometer for estimating the crystallization pressure of the monzogranites, the same has been attempted by a numerical method based on two polynomial equations:

$$P = -0.2426 \times (\mathrm{Qtz})^3 + 26.392 \times (\mathrm{Qtz})^2 - 980.74 \times (\mathrm{Qtz}) + 12563 \quad (1)$$

$$P = 0.2426 \times (\mathrm{Ab} + \mathrm{Or})^3 - 46.397 \times (\mathrm{Ab} + \mathrm{Or})^2 + 2981.3 \times (\mathrm{Ab} + \mathrm{Or}) - 64224 \quad (2)$$

$$(R^2 = 0.9943)$$

where, P is pressure in MPa, and R denotes correlation coefficient [52]. It is noted that the pressure is correlated respectively with normative quartz (Qtz) content and with normative albite (Ab) plus orthoclase (Or) contents of granitic rocks. Normalization of CIPW norm (quartz, albite, orthoclase) contents to 100% is required before using Equations (1) and (2). The difference in pressure calculations between these two equations is ≤16 MPa for the range of normative quartz contents from 15 to 40 wt%. Keeping this in mind for considering samples for calculation of crystallization pressure based on the two equations, the following pressures have been obtained. (**Table 5**)

The pressure difference in two equations varies from 8.025 MPa to 10.919 MPa which is within the range for normative quartz contents from 27.24% to 35.85%. Based on these results the crystallization pressure of the monzogranites can be estimated within 0.77 kbar to 5.51 kbar. Even though the range is quite high, but it gives an idea about the fact that the monzogranites have crystallized at lower pressures indicating lower depth of their formation than the granodiorites.

The high-temperature nature of granodiorites also suggest that they have been generated either in the lower crustal or upper mantle region (**Figure 19**). The heat required for melting the parent rocks at such high temperatures must be provided by the mantle-derived melts either directly or indirectly, *i.e.*, they may only provide the necessary heat for crustal melting or they may contribute mass through differentiation and assimilation of crustal melts [24]. The monzogranites have been generated from the crustal material. Thus, the I-type granodiorites have formed in volcanic arc setting by partial melting of the lower crust, promoted by heat from mantle-derived mafic melts producing a hybridized intermediate magma, that form granodiorite by fractional crystallization during its

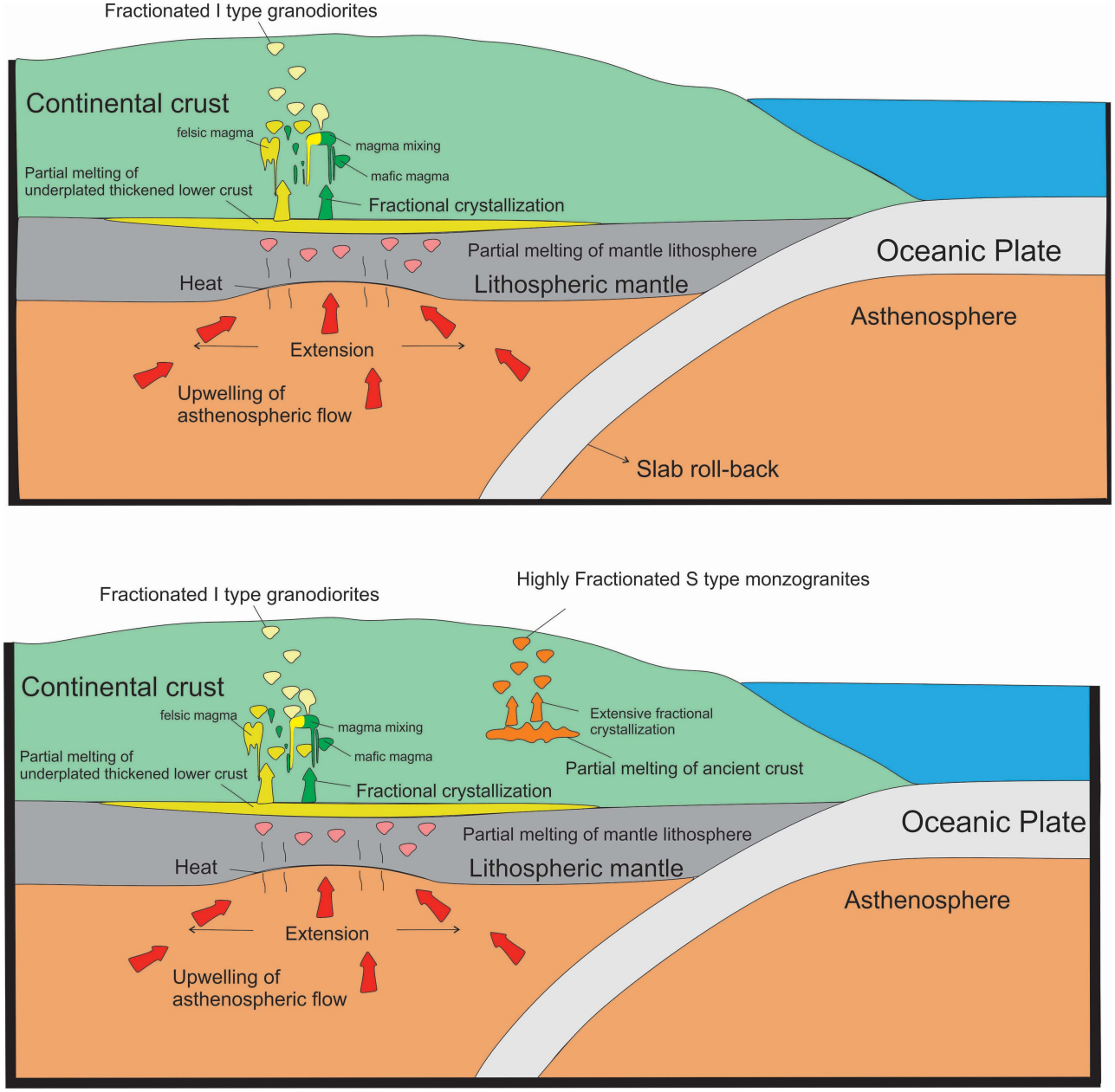

Figure 19. Cartoon illustration of the tectonic setting for the emplacement of granodiorites and the monzogranites.

Table 5. Average P calculated from normative Q, Ab and Or content in k-feldspar granites.

Sample id	Q	Or	Ab	P Qtz (MPa)	P (Ab + Or) (MPa)	Difference in P	Average P (MPa)	P (kbar)
PCS-12	35.65959	26.71066	37.62975	149.76104	141.27064	8.4904	145.51584	1.45516
PCS-13	26.89249	28.6314	44.47611	557.031187	546.11202	10.919163	551.5716	5.51572
PCS-20	34.93785	29.55898	35.50317	167.37343	158.73534	8.68809	163.05439	1.630544
PCS-14	29.19118	30.27346	40.53536	388.76305	378.61452	10.14853	383.68878	3.836889
BRS-30	38.33242	30.45524	31.21234	84.2255	76.200363	8.025137	80.212932	0.080213
BRS-31	38.44274	20.59154	40.96572	81.2487524	73.240056	8.008696	77.244404	0.772444
PCS-2	34.87812	29.46868	35.6532	168.86835	160.21762	8.650728	164.54298	1.64543
PCS-11	35.33194	33.11711	31.55096	157.667078	149.11079	8.556285	153.38894	1.53389
PCS-17	33.94665	29.4125	36.64085	193.309223	184.45303	8.56189	188.88113	1.88881
BRS-92	31.77476	33.47416	34.75107	263.68694	254.29102	9.395919	258.98898	2.58989

ascent and cooling [53]. This metaluminous magnesian-rich magma eventually produces subduction-related granodiorites. Ubiquitous presence of mafic micro granular magmatic enclaves (MME) with cuspate and lobate margins within the granodiorites suggests interaction and mixing/mingling of comagmatic mafic-felsic melts. The generation of the S-type monzogranites has been dominated by continental crust recycling due to continued orogenic activities and hydrothermal influx, rather than the addition of new material from mantle sources.

8. Conclusion

The area between the central and western arm of RSB, is characterized by different phases of granitoids with different tectonic histories. Migmatite gneiss rocks show mixed characters geochemically with complexly deformed nature observed in field and petrography. The granodiorites are formed from a hybridized intermediate magma by mixing of a mantle derived mafic melts with partially melted lower crust materials in the lower crustal or upper mantle region in a subduction region owing to their high emplacement temperature-pressure, numerous MMEs and high ∑REE content. These granodiorites are thus formed during the orogeny. The monzogranites have generated at shallower depth within the crust by continued crustal recycling owing to continued orogenic activities and hydrothermal influx in the subduction zone. The monzogranites have relatively low ∑REE content and highly fractionated REE pattern. Owing to the high hydrothermal influx in the monzogranites, these S-type peraluminous granites are rich in hydrothermal ore minerals viz., tungsten, tin, molybdenum, copper, etc.

Acknowledgements

The work has been carried out under Mineral Exploration- M-II G4 stage exploration programme of Geological Survey of India, State Unit: Andhra Pradesh, SR, Hyderabad during field season programme 2020-21. The authors gratefully

acknowledge Director General, Geological Survey of India, Addl. Director General and HOD, Geological Survey of India, Southern Region, Hyderabad for providing necessary facilities to carry out the work. The authors are extremely grateful to Shri. R.P. Nagar, Dy. Director General, State Unit: Andhra Pradesh, Southern Region, Hyderabad for his constructive suggestions during the course of work. The authors are thankful to the officers of Chemical Division and Petrology Division, Geological Survey of India, Southern Region, Hyderabad for analysis of the samples of granitoids collected during the field work. The authors are also indebted to the anonymous reviewers for their valuable scientific comments and suggestions.

Conflicts of Interest

The authors declare no conflicts of interest regarding the publication of this paper.

References

[1] Manikyamba, C. and Kerrich, R. (2012) Eastern Dharwar Craton, India: Continental Lithosphere Growth by Accretion of Diverse Plume and Arc Terranes. *Geoscience Frontiers*, **3**, 225-240. https://doi.org/10.1016/j.gsf.2011.11.009

[2] Ballal, N.R.R. (1970) Systematic Mapping in Parts of Dharmavaram and Penukonda Taluks, Anantapur District, Andhra Pradesh. Progress Report of Geological Survey of India.

[3] Kaul, B.L. and Sisodia, C.P. (1977) Systematic Geological Mapping in Parts of Penukonda, Dharmavaram and Hindupur Taluks of Anantapur District, Andhra Pradesh. Progress Report of Geological Survey of India of F.S. 1975-76.

[4] Rajesham, T. and Ramanaidu, K.V. (1995) Specialised Thematic Mapping of Peninsular Gneissic Complex vis-à-vis Supracrustals around Venkatampalle and Penakacherla Areas, in Parts of Anantapur District, Andhra Pradesh. *Extended Abstract*, *Records of the Geological Survey of India*, **129**, 12-15.

[5] Rajesham, T. and Vidyasagar, G. (1993) Geology of Parts of Anantapur District, Andhra Pradesh. *Extended Abstract*, *Records of the Geological Survey of India*, **127**, 13-15.

[6] Rajesham, T. and Kesari, G.K. (1993) Geology of Chennakothapalle Area, Anantapur District, Andhra Pradesh. *Extended Abstract*, *Records of the Geological Survey of India*, **126**, 18-20.

[7] Reddy, K.V.S., Vidyasagar, G. and Reddy, T.A. (1992) Geology of Atmakur and Kuderu Areas, Anantapur District, Andhra Pradesh. *Extended Abstract*, *Records of the Geological Survey of India*, **126**, 13-15.

[8] Reddy, K.V.S., Ramanaidu, K.V. and Reddy, T.A. (1993) Geology of Togarakunta-Perur Area, Anantapur District, Andhra Pradesh. *Extended Abstract*, *Records of the Geological Survey of India*, **127**, 10-12.

[9] Reddy, K.V.S. and Nayak, S.S. (1995) Specialised Thematic Mapping of Peninsular Gneissic Complex vis-à-vis Supracrustals in Parts of Anantapur District, Andhra Pradesh. *Extended Abstract*, *Records of the Geological Survey of India*, **129**, 9-12.

[10] Reddy, K.V.S. (1998) Compilation of STM Geological Maps of the Peninsular Gneissic Complex, Anantapur District, Andhra Pradesh. *Extended Abstract*, *Records of the Geological Survey of India*, **132**, 5-7.

[11] Suresh, G. and Viswanatha Rao, N. (1994) Study of Granitoids of Gooty-Singanamala Area, Anantapur District, Andhra Pradesh. *Extended Abstract*, *Records of the Geological Survey of India*, **128**, 6-7.

[12] Gopal Reddy, T., Viswanatha Rao, N. and Sarvothaman, H. (1992) Report on Granite Project. Progress Report of Geological Survey of India for F.S. 1988-90.

[13] Gopal Reddy, T. and Suresh, G. (1998) Classification and Characterization of the Peninsular Gneissic Complex in the Eastern Block of Dharwar Craton. *Indian Mineralogist*, **32**, 9-11.

[14] Gopal Reddy, T. and Suresh, G. (1993) Study of Granitic Rocks in Parts of Anantapur District, Andhra Pradesh. *Extended Abstract*, *Records of the Geological Survey of India*, **126**, 53-55.

[15] Gopal Reddy, T. and Suresh, G. (1994) Geological Studies on Granitoids and Associated Rocks of Kalyandurg-Atmakur-Anantapur Area, Anantapur District, Andhra Pradesh. Progress Report of Geological Survey of India for the F.S. 1991-92.

[16] Rajesham, T., Reddy, K.V.S., Ramanaidu, K.V., Nayak, S.S., Vidyasagar, G.V. and Kesari, G.K. (1998) Stratigraphy and Structure of the Ramagiri-Penakacherla Schist Belt of the Eastern Dharwar Craton, South India. *M.S. Krishnan Centenary Commemorative National Seminar on* 50 *Years of Progress in Precambrian Geology of India*, 142-143.

[17] Hanumanthu, R.C. and Babaiah, P.B. (1996) Origin of Granites Adjoining Ramagiri Schist Belt, Anantapur District, Andhra Pradesh. *Journal of the Geological Society of India*, **48**, 57-63.

[18] Sreenivas, B.L. and Srinivasan, R. (1974) Geochemistry of Granite-Greenstone Terrain of South India. *Journal of the Geological Society of India*, **15**, 390-406.

[19] Bouhallier, H., Choukroune, P. and Ballèvre, M. (1993) Diapirism, Bulk Homogeneous Shortening and Transcurrent Shearing in the Archaean Dharwar Craton: The Holenarsipur Area, Southern India. *Precambrian Research*, **63**, 43-58. https://doi.org/10.1016/0301-9268(93)90004-L

[20] Ohta, T. and Arai, H. (2007) Statistical Empirical Index of Chemical Weathering in Igneous Rocks: A New Tool for Evaluating the Degree of Weathering. *Chemical Geology*, **240**, 280-297. https://doi.org/10.1016/j.chemgeo.2007.02.017

[21] O'connor, J. (1965) A Classification for Quartz-Rich Igneous Rocks Based on Feldspar Ratios. US Geological Survey Professional Paper 525, 79-84.

[22] Irvine, T.N. and Baragar, W.R.A. (1971) A Guide to the Chemical Classification of Common Volcanic Rocks. *Canadian Journal of Earth Sciences*, **8**, 523-548. https://doi.org/10.1139/e71-055

[23] Whalen, J., Currie, K. and Chappell, B. (1987) A-Type Granites: Geochemical Characteristics, Discrimination and Petrogenesis. *Contributions to Mineralogy and Petrology*, **95**, 407-419. https://doi.org/10.1007/BF00402202

[24] Frost, B.R., Barnes, C.G., Collins. W.J., Arculus, R.J., Ellis, D.J. and Frost, C.D. (2001) A Geochemical Classification for Granitic Rocks. *Journal of Petrology*, **42**, 2033-2048. https://doi.org/10.1093/petrology/42.11.2033

[25] Middlemost, E.A.K. (1994) Naming Minerals in the Magma/Igneous Rock System. *Earth Science Reviews*, **37**, 215-224. https://doi.org/10.1016/0012-8252(94)90029-9

[26] De La Roche, H., Leterrier, J., Grandclaude, P. and Marchal, M. (1980) A Classification of Volcanic and Plutonic Rocks Using R1-R2 Diagram and Major Element Analyses. Its Relationships with Current Nomenclature. *Chemical Geology*, **29**, 183-210. https://doi.org/10.1016/0009-2541(80)90020-0

[27] Villaseca, C., Barbero, L. and Herreros, V. (1998) A Re-Examination of the Typology of Peraluminous Granite Types in Intracontinental Orogenic Belts. *Transactions of the Royal Society of Edinburgh. Earth Sciences*, **89**, 113-119. https://doi.org/10.1017/S0263593300007045

[28] Hastie, A.R., Kerr, A.C., Pearce, J.A. and Mitchell, S.F. (2007) Classification of Altered Volcanic Island Rocks Using Immobile Trace Elements: Development of the Th-Co Discrimination Diagram. *Journal of Petrology*, **48**, 2341-2357. https://doi.org/10.1093/petrology/egm062

[29] Peccerillo, A. and Taylor, S.R. (1976) Geochemistry of Eocene Calc Alkaline Volcanic Rocks from Kastamonu Area, Northern Turkey. *Contribution to Mineralogy and Petrology*, **58**, 63-81. https://doi.org/10.1007/BF00384745

[30] McDonough, W.F. and Sun, S.S. (1995) The Composition of the Earth. *Chemical Geology*, **120**, 223-253. https://doi.org/10.1016/0009-2541(94)00140-4

[31] Boynton, W.V. (1984) Cosmochemistry of the Rare Earth Elements: Meteorite Studies. In: Henderson, P., Ed., *Developments in Geochemistry*, Elsevier, Amsterdam, 63-114. https://doi.org/10.1016/B978-0-444-42148-7.50008-3

[32] Laurent, A., Janoušek, V., Magna, T., Schulmann, K. and Míková, J. (2014) Petrogenesis and Geochronology of a Post-Orogenic Calc-Alkaline Magmatic Association: The Žulová Pluton, Bohemian Massif. *Journal of Geosciences*, **59**, 415-440. https://doi.org/10.3190/jgeosci.176

[33] Maniar, P.D. and Piccoli, P. (1989) Tectonic Discrimination of Granitoids. *Geological Society of America Bulletin*, **101**, 635-643. https://doi.org/10.1130/0016-7606(1989)101<0635:TDOG>2.3.CO;2

[34] Shand, S.J. (1943) The Eruptive Rocks. 2nd Edition, John Wiley, New York, 444.

[35] Pearce, J.A., Harris, N.B.W. and Tindle, A.G. (1984) Trace Element Discrimination Diagrams for the Tectonic Interpretation of Granitic Rocks. *Journal of Petrology*, **25**, 956-983. https://doi.org/10.1093/petrology/25.4.956

[36] Pearce, J.A. (1996) Sources and Settings of Granitic Rocks. *Episode*, **19**, 120-125. https://doi.org/10.18814/epiiugs/1996/v19i4/005

[37] Batchelor, R.A. and Bowden, P. (1985) Petrogenetic Interpretation of Granitoid Rock Series Using Multicationic Parameters. *Chemical Geology*, **48**, 43-55. https://doi.org/10.1016/0009-2541(85)90034-8

[38] Pitcher, W.S. (1983) Granite Type and Tectonic Environment. In: Hsu, K., Ed., *Mountain Building Processes*, Academic Press, London, 19-40.

[39] Leake, B.E., Wooley, A.R., Arps, C.E.S., Birch, W.D., Gilbert, M.C., Grice, J.D., Hawthorne, F.C., Kato, A., Kisch, H.J., Krivovichev, V.G., Linthout, K., Laird, J., Mandarino, J.A., Maresch, W.V., Nickel, E.H., Rock, N.M.S., Schumacher, J., Smith, J.C., Stephenson, N.C.N. Whittaker, E.J.W. and Youzhi, G. (1997) Nomenclature of Amphiboles: Report of the Subcommittee on Amphiboles of the International Mineralogical Association Commission on New Minerals and Mineral Names. *Mineralogical Magazine*, **61**, 295-321. https://doi.org/10.1180/minmag.1997.061.405.13

[40] Hawthorne, F.C., Oberti, R., Harlow, G.E., Maresch, W.V., Martin, R.F., Schumacher, J.C. and Welch, M.D. (2012) IMA Report. Nomenclature of the Amphibole Supergroup. *American Mineralogist*, **97**, 2031-2048. https://doi.org/10.2138/am.2012.4276

[41] Watson, E.B. and Harrison, M. (1983) Zircon Saturation Revisited: Temperature and Composition Effects in a Variety of Crustal Magma Types. *Earth and Planetary Science Letters*, **64**, 295-304. https://doi.org/10.1016/0012-821X(83)90211-X

[42] Miller, C.F., Meschter, S., Dowell, M. and Mapes, R.W. (2003) Hot and Cold Granites? Implication of Zircon Saturation Temperatures and Preservation of Inheritance. *Geology*, **31**, 529-532. https://doi.org/10.1130/0091-7613(2003)031<0529:HACGIO>2.0.CO;2

[43] Hammarstron, J.M. and Zen, E.A. (1986) Aluminium in Hornblende: An Empirical Igneous Geobarometer. *American Mineralogist*, **71**, 1297-1313.

[44] Hollister, L.S., Grisson, G.C., Peters, E.K., Stowell, H.H. and Sisson, V.B. (1987) Confirmation of the Empirical Correlation of Al in Hornblende with Pressure of Solidification of Calc-Alkaline Plutons. *American Mineralogist*, **72**, 231-239.

[45] Johnson, M.C. and Rutherford, M.J. (1989) Experimental Calibration of the Aluminium in Hornblende Geobarometer with Application to Long Valley Caldera (California) Volcanic Rocks. *Geology*, **17**, 837-841. https://doi.org/10.1130/0091-7613(1989)017<0837:ECOTAI>2.3.CO;2

[46] Thomas, W. and Ernst, W.G. (1990) The Aluminum Content of Hornblende in Calcalkaline Granitic Rocks; a Mineralogic Barometer Calibrated Experimentally to 12 kbars. In: Spencer, R.J. and Chou, I.-M., Eds., *Fluid-Mineral Interactions*: *A Tribute to H.P. Eugster*, *Geochemical Society Special Publications*, Geochemical Society, Washington DC, Vol. 2, 59-63.

[47] Schmidt, M.W. (1992) Amphibole Composition in Tonalite as a Function of Pressure: An Experimental Calibration of the Al-in-Hornblende Barometer. *Contributions to Mineralogy and Petrology*, **110**, 304-310. https://doi.org/10.1007/BF00310745

[48] Mutch, E.J.F., Blundy, J.D., Tattitch, B.C., Cooper, F.J. and Brooker, R.A. (2016) An Experimental Study of Amphibole Stability in Low-Pressure Granitic Magmas and a Revised Al-in-Hornblende Geobarometer. *Contributions to Mineralogy and Petrology*, **171**, 85. https://doi.org/10.1007/s00410-016-1298-9

[49] Stein, E. and Dietl, E. (2001) Hornblende Thermobarometry of Granitoids of Central Odenwald (Germany) and Their Implication for the Geotectonic Development of the Odenwald. *Mineralogy and Petrology*, **72**, 185-207. https://doi.org/10.1007/s007100170033

[50] Leake, B.E. (1978) Nomenclature of Amphiboles. *American Mineralogist*, **63**, 1023-1052.

[51] Agemar, T., Worner, G. and Heumann, A. (1999) Stable Isotopes and Amphibole Chemistry on Hydrothermally Altered Granitoids in the North Chilean Precordillera: A Limited Role for Meteoric Water? *Contributions to Mineralogy and Petrology*, **136**, 331-344. https://doi.org/10.1007/s004100050542

[52] Yang, X.-M. (2017) Estimation of Crystallization Pressure of Granite Intrusions. *Lithos*, **286-287**, 324-329. https://doi.org/10.1016/j.lithos.2017.06.018

[53] Abdelfadil, K.M., Obeid, M.A., Azer, M.K. and Asimow, P.D. (2018) Late Neoproterozoic Adakitic Lavas in the Arabian-Nubian Shield, Sinai Peninsula Egypt. *Journal of Asian Earth Sciences*, **158**, 301-323. https://doi.org/10.1016/j.jseaes.2018.02.018